



**HAL**  
open science

## **Iron isotope fractionation in iron-organic matter associations: Experimental evidence using filtration and ultrafiltration**

Elaheh Lotfi-Kalahroodi, Anne-Catherine Pierson-Wickmann, H el ene Gu enet, Olivier J. Rouxel, Emmanuel Ponzevera, Martine Bouhnik-Le Coz, Delphine Vantelon, Aline N. Dia, M elanie Davranche

### **► To cite this version:**

Elaheh Lotfi-Kalahroodi, Anne-Catherine Pierson-Wickmann, H el ene Gu enet, Olivier J. Rouxel, Emmanuel Ponzevera, et al.. Iron isotope fractionation in iron-organic matter associations: Experimental evidence using filtration and ultrafiltration. *Geochimica et Cosmochimica Acta*, 2019, 250, pp.98-116. 10.1016/j.gca.2019.01.036 . insu-02008998

**HAL Id: insu-02008998**

**<https://insu.hal.science/insu-02008998>**

Submitted on 6 Feb 2019

**HAL** is a multi-disciplinary open access archive for the deposit and dissemination of scientific research documents, whether they are published or not. The documents may come from teaching and research institutions in France or abroad, or from public or private research centers.

L'archive ouverte pluridisciplinaire **HAL**, est destin ee au d ep ot et  a la diffusion de documents scientifiques de niveau recherche, publi es ou non,  emanant des  tablissements d'enseignement et de recherche fran ais ou  trangers, des laboratoires publics ou priv es.

## Accepted Manuscript

Iron isotope fractionation in iron-organic matter associations: Experimental evidence using filtration and ultrafiltration

Elaheh Lotfi-Kalahroodi, Anne-Catherine Pierson-Wickmann, H el ene Gu enet, Olivier Rouxel, Emmanuel Ponzevera, Martine Bouhnik-LeCoz, Delphine Vantelon, Aline Dia, M elanie Davranche

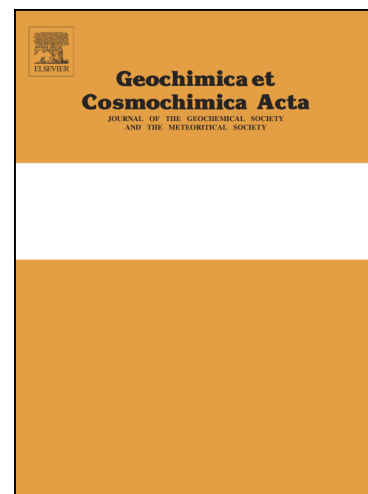
PII: S0016-7037(19)30060-2  
DOI: <https://doi.org/10.1016/j.gca.2019.01.036>  
Reference: GCA 11109

To appear in: *Geochimica et Cosmochimica Acta*

Received Date: 4 April 2018  
Revised Date: 29 November 2018  
Accepted Date: 23 January 2019

Please cite this article as: Lotfi-Kalahroodi, E., Pierson-Wickmann, A-C., Gu enet, H., Rouxel, O., Ponzevera, E., Bouhnik-LeCoz, M., Vantelon, D., Dia, A., Davranche, M., Iron isotope fractionation in iron-organic matter associations: Experimental evidence using filtration and ultrafiltration, *Geochimica et Cosmochimica Acta* (2019), doi: <https://doi.org/10.1016/j.gca.2019.01.036>

This is a PDF file of an unedited manuscript that has been accepted for publication. As a service to our customers we are providing this early version of the manuscript. The manuscript will undergo copyediting, typesetting, and review of the resulting proof before it is published in its final form. Please note that during the production process errors may be discovered which could affect the content, and all legal disclaimers that apply to the journal pertain.



**Iron isotope fractionation in iron-organic matter associations:  
Experimental evidence using filtration and ultrafiltration**

Elaheh Lotfi-Kalahroodi<sup>1\*</sup>, Anne-Catherine Pierson-Wickmann<sup>1</sup>, H el ene Gu enet<sup>1</sup>, Olivier Rouxel<sup>2,3</sup>, Emmanuel Ponzevera<sup>2</sup>, Martine Bouhnik-LeCoz<sup>1</sup>, Delphine Vantelon<sup>4</sup>, Aline Dia<sup>1</sup> and M elanie Davranche<sup>1</sup>

<sup>1</sup> Univ. Rennes, CNRS, G eosciences Rennes - UMR 6118, F-35000 Rennes, France

<sup>2</sup> IFREMER, Unit e de G eosciences Marines, 29280 Plouzan e, France

<sup>3</sup> Univ. Hawaii, Department of Oceanography, Honolulu, HI 96822, USA

<sup>4</sup> Synchrotron SOLEIL, L'orme des merisiers, Saint Aubin BP48, 91192, Gif sur Yvette Cedex, France

*In revision to Geochimica et Cosmochimica Acta*

**\*Corresponding author: [elaheh.lotfi-kalahroodi@univ-rennes1.fr](mailto:elaheh.lotfi-kalahroodi@univ-rennes1.fr)**

**Abstract** — Colloids have been recognized as key vectors of pollutants in aqueous environment. Amongst them, those formed by iron (Fe) and organic matter (OM) are of major importance due to their ubiquity in the surface environment and strong affinity for metals. In the recent years, Fe stable isotopes have been increasingly used to elucidate the sources and biogeochemical cycling of Fe in Earth's surface environments. In this study, we aim to elucidate (i) the possible Fe isotopic signature resulting from the Fe/OM colloid formation and (ii) the mechanisms involved in the development of such isotopic signature. For this purpose, Fe-OM associations were synthesized through binding and titration experiments. Various pH levels were used in order to study the isotope behavior of Fe occurring as free species at pH 1, as Fe-OM complexes at pH 2 and as mixed Fe-oxyhydroxide/OM nanoaggregates or particles at pH 6.5. Organic matter-free, Fe-free and OM membrane-deposition experiments were also performed. These suspensions were (ultra)filtered at 0.2  $\mu\text{m}$ , 30 kDa and 5 kDa to

evidence the possible Fe isotope fractionation between fractions. This protocol allowed also testing the potential of (ultra)filtration techniques to generate isotope fractionation. The results provided evidence that abiotic Fe precipitation, (ultra)filtration techniques and OM deposition were not able to produce significant Fe isotope fractionation under the experimental conditions. However, at circum-neutral pH, the Fe-OM binding and titration experiments displayed a significant enrichment of heavy Fe isotopes in the < 30 kDa fractions relative to the total Fe pool  $\delta^{56}\text{Fe} = 0.35 \pm 0.05\text{‰}$  and  $0.26 \pm 0.05\text{‰}$  (95% confidence interval,  $2\sigma$  and relative to international standard IRMM-14), respectively. Mass balance and error propagation calculation showed Fe isotope fractionation in binding and titration experiments between the > 30 kDa and < 30 kDa fractions for  $-0.35 \pm 0.05\text{‰}$  and  $-0.27 \pm 0.05\text{‰}$ , respectively. This Fe isotope fractionation could be due to the complexation of Fe by OM in the < 30 kDa fractions. At pH 2, the OM-free experiment, the < 30 kDa fraction showed Fe isotope ratio  $\delta^{56}\text{Fe} = 0.75 \pm 0.03\text{‰}$  with an enrichment in heavy Fe isotopes of  $\delta^{56}\text{Fe}' = 0.14 \pm 0.04\text{‰}$  relative the total Fe pool ( $\delta^{56}\text{Fe}'$  is  $\delta^{56}\text{Fe}$  value which was corrected by  $\delta^{56}\text{Fe}$  of total fraction). This enrichment in heavy Fe isotopes induced an isotopic fractionation factor of  $-0.87 \pm 0.26\text{‰}$  between the > 30 kDa and < 30 kDa fractions produced by the complexation between the heavy Fe isotopes and  $\text{OH}^-$  ligands in the < 30 kDa fraction. Natural Fe-OM associations were further investigated through oxidation experiments of a reduced wetland soil solution. The oxidized soil solution was (ultra)filtered at 5  $\mu\text{m}$ , 3  $\mu\text{m}$ , 0.2  $\mu\text{m}$ , 30 kDa and 5 kDa. The highest  $\delta^{56}\text{Fe}$  was obtained in the smallest size fraction, i.e. < 5 kDa fraction, yielding a negative isotopic fractionation  $\Delta^{56}\text{Fe}_{>5\text{kDa} - <5\text{kDa}} = -0.23 \pm 0.08\text{‰}$  suggesting that Fe heavy isotopes are preferentially bound to small humic OM molecules in the form of Fe monomers or small clusters. This study highlights the importance of organic matter for metals' isotopic systems.

### Keywords

*Filtration, size fractionation, isotope fractionation, colloidal, dissolved, Fe isotopes*

## 1. INTRODUCTION

Iron (Fe) cycle is of major importance in the control of the environmental behavior of many chemical organic or inorganic elements. In aquatic surface environments, Fe can be distributed between truly dissolved, colloidal and particulate fractions, with a strong control of physico-chemical conditions (pH, Eh, etc) and organic and inorganic ligands (Pokrovsky and Schott, 2002; Allard et al., 2004; Liang et al., 2005; Sigg et al., 2014; dos Santos Pinheiro et al., 2014). In surface waters, groundwaters and soil solutions, Fe is largely present as colloids or nano-aggregates in which Fe(III) is often bound to organic matter (OM) (Pokrovsky et al., 2005; Guénet et al., 2016; Guénet et al., 2017). Such colloids are produced via anthropogenic forcing, physical and geochemical processes such as, alteration or erosion, and redox cycles resulting from water saturation/desaturation of soils (Chen et al., 2014; Hirst et al., 2017). Their production actually increases in response to the environmental changes associated with an increase in the frequency and intensity of rainfall and permafrost thawing (Shirokova et al., 2013; Manasyrov et al., 2015). Such Fe-rich colloids are strong sorbents of contaminants (organic or inorganic) and subsequently key vectors of pollutants (e.g. Pédrot et al., 2008). The increase of their production, natural or not, can have dramatic consequences for the water and soil quality. Recently, Guénet et al. (2017) demonstrated that the structural arrangement of Fe-OM colloids, controls their metal(loid) binding capacity which is dependent of their Fe/OM ratio rather than the specific surface area. Under environmental conditions, the Fe/OM ratio depends on the physico-chemical conditions prevailing during colloid formation. The most important parameters are the redox conditions, the pH and the OM properties. Elucidating the impact of such parameters on the colloids formation is therefore crucial but not trivial. Several characterization approaches could be used, for example, (i) fine structural characterization techniques such as X-ray absorption spectroscopy (XAS), small-angle X-ray scattering SANS or Small-angle X-ray scattering (SAXS), (Guénet et al., 2017) and (ii) the variation of the Fe isotopic signature (expressed as  $\delta^{56}\text{Fe}$  or  $\delta^{57}\text{Fe}$  relative to international standard IRMM-14). Iron isotopic fractionation has been shown to be able to trace biogeochemical processes and iron sources modern in Earth's surface environment (Bullen et al., 2001; Welch et al., 2003; Wiederhold et al., 2007; Johnson et al., 2008; Dauphas et al., 2017; Abadie et al., 2017). The principal mechanisms expected to fractionate Fe isotope ratios include (i) abiotic Fe(II) oxidation and isotope exchange between Fe(II) and

Fe(III) (Welch et al., 2003), (ii) bacteria-mediated Fe(II) oxidation (e.g. Croal et al., 2004), (iii) bacteria-mediated Fe(III) reduction (Icopini et al., 2004; Crosby et al., 2007) (iv) complexation by organic ligand (Dideriksen et al., 2008; Morgan et al., 2010) (v) Fe(II) sorption onto Fe(III) oxyhydroxides (Teutsch et al., 2005; Frierdich et al., 2014) and (vi) precipitations of ferric oxyhydroxides (Johnson et al., 2002; Wu et al., 2012). To be able to investigate Fe isotope composition of colloids under natural conditions (rivers, estuaries, etc.), several studies used ultrafiltration separation techniques. In boreal waters, Ilina et al. (2013) reported that  $\delta^{57}\text{Fe}$  increases with the decreasing Fe/ $C_{\text{org}}$  molar ratio while a reverse trend was observed by Schroth et al. (2011) and Escoube et al. (2015) in OM-rich colloids from high-latitude streams and meltwater due to active redox cycling. In estuaries, the flocculation of humic acid-rich colloids is a well-known process (Sholkovitz, 1976). Escoube et al. (2009) and Rouxel and Auro, (2010) showed that colloid flocculation in estuaries produces insignificant Fe isotope fractionation. These observations were only possible thanks to the use of the size fractionation method allowing the discrimination of the prevailing chemical processes between dissolved and particulate Fe pools. However, several studies suggested that (ultra)filtration techniques may induce analytical artifacts in response to charge separation, diffusion, or filter clogging by OM (Ilina et al., 2013; Escoube et al., 2015).

It is recognized that Fe is almost present as Fe/OM nanoaggregates in circum-neutral pH natural waters (e.g. Allard et al., 2004) which exert a major control on Fe isotope composition in streams and rivers water (Ilina et al., 2013; Escoube et al., 2015). The exact control of Fe isotope composition in different colloidal sizes remains poorly known, and it is often difficult to disentangle source effects (i.e. different Fe pools having different origins) from isotope fractionation effects (i.e. different Fe pools undergoing Fe isotope exchange among them). As a consequence, the aim of this study was to elucidate the mechanisms involved in the Fe isotope fractionation resulting from the formation of Fe/OM nano-associations, and shed new light on the application of Fe isotope systematics of aqueous and weathering environments. We therefore designed experiments to produce synthetic Fe-OM associations and decipher the resulting Fe isotopic fractionation. This study focuses on the most reactive part of OM encountered in natural environments, i.e. humic substances. The Fe/OM nanoaggregates were synthesized under abiotic conditions through a Fe-OM binding and an OM titration by Fe experiments. Several pH were tested to be able to establish a range of Fe

speciation in solution, allowing to determine the possible Fe isotope fractionation factors among several Fe pools when Fe was present as free species (pH 1), as Fe-OM complexes (pH 2) and as mixed Fe-oxyhydroxide/OM nanoaggregates or particles (pH 6.5). The various chemical species for each synthesis methodology were size-separated by using (ultra)filtration at decreasing pore size (0.2  $\mu\text{m}$ , 30 kDa and 5 kDa). This protocol allowed also testing whether or not ultrafiltration introduced spurious Fe isotopic fractionation. Finally, the Fe isotopic composition of "natural" Fe-OM associations was investigated using oxidation by-products of a reduced soil solution.

## 2. MATERIAL AND METHODS

All of the chemicals used in this study were of analytical grade. The solutions were prepared with ultrapure 18 M $\Omega$  water (Milli-Q system, Millipore). The containers used were (i) cleaned with 10% (v/v) HNO<sub>3</sub> for 24 h at 45°C (ii) and then with ultrapure water for 24 h at 45°C, and (iii) finally dried at 30°C. For sample digestion and chromatographic separation, analytical grade nitric and hydrofluoric acids were further purified by triple sub-boiling distillation in PFA vessel. Hydrochloric acid was purified in a PFA acid purification system (DST-1000, Savillex). The organic matter stock solution at 83 mmol L<sup>-1</sup> of dissolved organic carbon (DOC), hereafter referred to as "OM solution", was made by dissolving 2 g of Gascoyne Leonardite soil (Cat. No. BS104L) obtained from the International Humic Substances Society (IHSS) (C = 49.2%, H = 4.5% and N = 0.9% as a mass fraction) in ultrapure water. All of the experiments were performed in duplicate. The samples were filtered through a 0.2  $\mu\text{m}$  pore-size cellulose acetate membrane (Sartorius®), previously washed with ultrapure water. Roughly 15 mL of the aliquot was also processed by ultrafiltration at 30 kDa and 5 kDa (Vivaspin®, Sartorius) by centrifugation at 2790 g for 15 min and 2790 g for 30 min, respectively. The 30 kDa and 5 kDa ultrafiltration cells were previously cleaned using ultrapure water. At least 97% of sample was recovered. The procedural blank of (ultra)filtration membranes was assessed by processing ultrapure water throughout the entire filtration and ultrafiltration steps and Fe concentrations were not significant for our results (below 40 nmol L<sup>-1</sup>). The iron concentration in the blanks never exceeded 6.7 % of the minimum amount of Fe processed through the experiment.

## 2.1. Fe-OM binding experiments

Iron binding experiments were performed by mixing 250 mL of OM solution at 4.2 mmol L<sup>-1</sup> of dissolved organic carbon with a Fe(NO<sub>3</sub>)<sub>3</sub>·9H<sub>2</sub>O solution at 89 μmol L<sup>-1</sup> of Fe to obtain a Fe/C<sub>org</sub> (mol./mol.) ratio of 0.02, within the range of the calculated ratios in the soil solution in the Kervidy-Naizin wetland (France) (OZCAR Environmental Research Infrastructure) (Davranche *et al.*, 2013; Lambert *et al.*, 2014). This Fe/C<sub>org</sub> is comparable with that at 0.01 for a soil solution of a Russian swamp zone (Pokrovsky *et al.*, 2005) and at 0.006 for a water stream in a German wetland (Neubauer *et al.*, 2013). The ionic strength (IS) was fixed at 1 mmol L<sup>-1</sup> with NaNO<sub>3</sub> electrolyte solution. The experimental pH was adjusted to pH 1, 2 and 6.5 using ultrapure HNO<sub>3</sub> or analytical grade NaOH. The pH 6.5 corresponds to typical pH encountered in soil solutions, whereas the pH 1 was chosen to ensure that Fe remains as free species and pH 2 was set to produce dissolved Fe complexes and to prevent Fe precipitation. The solutions were stirred for 24 h to reach a steady state as in previous studies (Weber *et al.*, 2006; Catrouillet *et al.*, 2014). Then the suspensions were filtered through a 0.2 μm and ultrafiltered at 30 and 5 kDa. The Fe isotopic ratio (δ<sup>56</sup>Fe and δ<sup>57</sup>Fe) and Fe concentrations were analyzed for the total fraction as well as the < 0.2 μm, < 30 kDa and < 5 kDa fractions.

## 2.2. Organic matter titration by Fe

Approximately 247 mL of OM solution at 4.2 mmol L<sup>-1</sup> DOC were titrated with a solution of Fe(NO<sub>3</sub>)<sub>3</sub> at 8.9 mmol L<sup>-1</sup> of Fe(III) at 0.05 mL min<sup>-1</sup> using the first automated titrator (Titrino 794, Metrohm). The second titrator using a pH state mode (Titrino 794, Metrohm) provided the OH<sup>-</sup> for the Fe hydrolysis reaction through an electrolyte solution of 100 mmol L<sup>-1</sup> NaOH to keep the pH constant (Guénet *et al.*, 2017). The accuracy of the pH measurement was ±0.04 pH unit. At the end of the titration, the suspensions were filtered at 0.2 μm and 15 mL of filtrate were also ultrafiltered at 30 and 5 kDa. The Fe isotopic values and Fe concentrations were analyzed for the total fraction as well as the < 0.2 μm, < 30 kDa and < 5 kDa fractions.

Iron-OM binding experiment was performed by a rapid mixing of Fe with OM to promote the formation of Fe-OM complexes rather than colloids. By contrast, the titration of OM by Fe

was performed to promote the formation of large Fe-OM aggregates rather than Fe-OM complexes. During titration, the Fe hydrolysis is indeed improved by the constant NaOH addition.

### 2.3. Organic matter deposition experiment

An organic matter deposition experiment was conducted to test the potential impact of the partially coated (ultra)filtration membrane with OM on both the recovery of Fe in the filtrate and its Fe isotopic composition. The experiment was performed in two steps. Organic matter solution at  $8.4 \text{ mmol L}^{-1}$  DOC was filtered at  $0.2 \mu\text{m}$ . An aliquot of filtrate was ultrafiltered at 30 and 5 kDa. Each (ultra)filtration at  $0.2 \mu\text{m}$ , 30 kDa and 5 kDa resulted on the OM deposition on the membrane. Then,  $0.18 \text{ mmol L}^{-1}$  of Fe(III) solution was filtered through each membrane partially coated by OM. This experiment was performed at pH 2 and 6.5 with a target  $\text{Fe}/C_{\text{org}} = 0.02$ . The Fe concentrations and isotopic ratios were analyzed for the total fraction as well as the  $< 0.2 \mu\text{m}$ ,  $< 30 \text{ kDa}$  and  $< 5 \text{ kDa}$  fractions.

### 2.4. Production of 'natural' Fe-OM associations

Natural Fe-OM associations were produced from a reduction/oxidation experiment of a soil solution. The soil was sampled in the organo-mineral horizon of the planosol of the Mercy wetland (Brittany, France) (Grybos *et al.*, 2007). The soil was first incubated under anoxic conditions in a Jacomex<sup>®</sup> anaerobic chamber. Approximately 130 g of sieved moist soil (at 2 mm and soil moisture = 44 wt.%) was mixed with 1.8 L of a solution prepared with  $0.48 \text{ mmol L}^{-1}$  of  $\text{NaNO}_3$  and  $\text{NaCl}$ , and  $0.1 \text{ mmol L}^{-1}$  of  $\text{Na}_2\text{SO}_4$  (Guénet *et al.*, 2017). This solution mimics the anionic composition of autumnal water when the water level increases in the wetland (Grybos *et al.*, 2007). Anoxic incubations were performed in triplicate. The reduction progress was followed through the increase in the pH and Fe(II) concentrations (reaching 7.2 and  $0.52 \text{ mmol L}^{-1}$ , respectively) and the decrease in the Eh values (reaching approximately -130 mV). The soil suspensions were first filtered through  $5 \mu\text{m}$  cellulose nitrate filters (Sartorius<sup>®</sup>). The soil solutions were split into three parts and stored in contact with ambient air in a dark room for 2 weeks to ensure extensive Fe(II) oxidation (as shown by XANES records, Guénet *et al.*, 2017). Using the same experimental setup, a previous study

showed that Fe(II) is oxidized in less than 10 min and an apparent steady state was reached in the size redistribution between particles and colloids (Guénet *et al.*, 2017). The solutions were then filtered in a cascade mode using cellulose nitrate membrane filters at 5  $\mu\text{m}$ , 3  $\mu\text{m}$  and 0.2  $\mu\text{m}$  (Sartorius filters). The < 0.2  $\mu\text{m}$  fraction was then ultrafiltered at 30 kDa and 5 kDa using a Labscale TFF system equipped with two Pellicon XL membranes (PXC030C50 and PXC05C50).

## 2.5. Chemical analyses

The dissolved organic carbon concentration was determined using a total carbon analyzer (Shimadzu TOC-V CSH) with an uncertainty of 5% by a standard solution of potassium hydrogen phthalate (Sigma Aldrich). For the purpose of the trace element analysis, acidified filtrate samples were evaporated and pre-digested twice with 14.6 mol L<sup>-1</sup> distilled HNO<sub>3</sub> at 90°C to release Fe from the organic complexes. The second step of digestion was performed using a mixture of 1 mL of 30% H<sub>2</sub>O<sub>2</sub> and 2 mL of 14.6 mol L<sup>-1</sup> HNO<sub>3</sub> to eliminate the OM. After total evaporation, they were then dissolved in 0.37 mol L<sup>-1</sup> HNO<sub>3</sub>. The Fe concentration analysis was carried out using an Agilent 7700X inductively coupled plasma mass spectrometer (ICP-MS) at Geosciences Rennes (University of Rennes) with precision of 3% and 5% for > and < 1.8  $\mu\text{mol L}^{-1}$  of Fe, respectively.

## 2.6. Iron purification

Acidified samples (roughly 15 mL of solutions, corresponding to no more than 100  $\mu\text{g}$  or 1.79  $\mu\text{mol}$  of Fe, (Rouxel *et al.*, 2008) were digested overnight in PFA vials containing 3 mL of 14.6 mol L<sup>-1</sup> HNO<sub>3</sub> and 0.5 mL of 22.6 mol L<sup>-1</sup> HF and placed on a hot plate at 90°C. After complete evaporation, the samples were further digested overnight with 2 mL of 14.6 mol L<sup>-1</sup> HNO<sub>3</sub> and 1 mL of 12 mol L<sup>-1</sup> HCl. After evaporation to dryness, they were then dissolved with 1 mL of suprapure 30% H<sub>2</sub>O<sub>2</sub> and 2 mL of 14.6 mol L<sup>-1</sup> HNO<sub>3</sub> and digested for 24 h at 90°C in closed PFA vials. Then, they were evaporated to dryness again. These steps were done to release Fe from the organic and inorganic compounds. The samples were then dissolved in 2 mL of 5 mol L<sup>-1</sup> HCl and 30  $\mu\text{L}$  of 30% H<sub>2</sub>O<sub>2</sub> to ensure that Fe was completely present as Fe(III) in the solution before loading on the resin. Iron purification was achieved by

ion chromatography using the anion exchange resin Dowex® 1X8, chloride form (100-200 mesh). The chromatography columns were filled with 2 mL of resin, cleaned and conditioned by running 10 mL of ultrapure H<sub>2</sub>O, 10 mL of 3 mol L<sup>-1</sup> HNO<sub>3</sub>, 10 mL of H<sub>2</sub>O, 5 mL of 0.24 mol L<sup>-1</sup> HCl and 5 mL of 5 mol L<sup>-1</sup> HCl. The sample solutions were loaded in 2.0 mL of 5 mol L<sup>-1</sup> HCl with trace of 30% H<sub>2</sub>O<sub>2</sub>. Then, 15 mL of 5 mol L<sup>-1</sup> HCl was passed through the column in 2.5 mL increments to remove the matrix elements. Finally, Fe was eluted using 12 mL of 0.24 mol L<sup>-1</sup> HCl and collected in 15 mL PFA vials. The purified Fe solution was evaporated to dryness and the residue was dissolved in 0.28 mol L<sup>-1</sup> of HNO<sub>3</sub> for mass spectrometry analysis.

Procedural blanks, including evaporation/digestion and ion exchange purification steps were determined for each sample batch. These blanks contained on average  $0.47 \pm 0.4$  nmol of Fe. Compared to typical amount of Fe processed through the entire purification steps within the range of 30.4 nmol to 52.5  $\mu$ mol, the blanks represent less than 1.6 % of Fe and therefore insignificant. An internal standard BHVO-1 (a Hawaiian basalt) with an average Fe isotopic composition of  $\delta^{56}\text{Fe}$  of  $0.10 \pm 0.09\text{‰}$  (2SD) (Rouxel *et al.*, 2008) was used to evaluate the accuracy of the method. The yields from the sample purification steps were also verified by measuring the residual concentration of Fe in the eluted matrix solution using a ferrozine assay (Stookey, 1970; Jeitner, 2014). In all cases, the Fe concentrations were below the detection limits, suggesting that less than 1% of Fe was lost during the purification (i.e. recovery > 99%).

## 2.7. Iron isotope measurements

Iron isotope composition analyses were performed at IFREMER in Brest (France) using a Thermo Neptune-plus multicollector inductively coupled plasma mass spectrometer (MC-ICP-MS) following the method described in Rouxel *et al.* (2008). Solutions were introduced into the MC-ICPMS using a cyclonic spray chamber and a low-flow pneumatic nebulizer at 60  $\mu\text{L}\cdot\text{min}^{-1}$ . For sample solutions with Fe concentrations below 5.4 nmol L<sup>-1</sup>, a desolvation nebulizer (Cetac Apex) was used to improve instrumental sensitivity.

The Neptune instrument was equipped with high-sensitivity X-cones and was operated in either high or medium mass resolution to resolve argon-based interferences on Fe isotopes. The cups were configured to measure <sup>52</sup>Cr, <sup>54</sup>Fe, <sup>56</sup>Fe, <sup>57</sup>Fe, <sup>58</sup>Fe, <sup>60</sup>Ni, <sup>61</sup>Ni and <sup>62</sup>Ni in dynamic mode. This setup allows the correction of <sup>54</sup>Cr interference on <sup>54</sup>Fe using <sup>52</sup>Cr abun-

dances and the measurement of the  $^{62}\text{Ni}/^{60}\text{Ni}$  ratios for instrumental mass bias corrections. In addition, a sample-standard bracketing approach was applied, using the IRMM-14 international reference material and a SPEX internal standard solution. A Ni reference solution was added to the standards and samples with a Ni/Fe ratio of 1 g/g.

In general, the Fe isotope compositions were measured at a concentration ranging from 18 to 72  $\mu\text{mol L}^{-1}$  with a maximum difference of less than 10% between the concentrations of the samples and the standard. In the literature, the measured concentrations varied from 0.9 to 89  $\mu\text{mol L}^{-1}$  (Rouxel *et al.*, 2008; Escoube *et al.*, 2009).

Isotopic data are reported in delta notation relative to the IRMM-014 standard, expressed as  $\delta^{56}\text{Fe}$ , which represents the deviation in per mil relative to the reference material:

$$\delta^{56}\text{Fe}(\text{‰}) = \left( \frac{(^{56}\text{Fe}/^{54}\text{Fe})_{\text{sample}}}{(^{56}\text{Fe}/^{54}\text{Fe})_{\text{IRMM-014}}} - 1 \right) * 1000 \quad (\text{Eq. 1})$$

Since the total Fe fraction used in our experiments fractionated  $\delta^{56}\text{Fe}$  values relative to IRMM-14 (about 0.5 ‰), we introduce another notation ( $\delta^{56}\text{Fe}'$ ). It corresponds to the Fe isotope composition of the different Fe fractions ( $\delta^{56}\text{Fe}_A$ ) corrected from the total Fe isotope composition ( $\delta^{56}\text{Fe}_{\text{Total}}$ ), such as:

$$\delta^{56}\text{Fe}'_A(\text{‰}) = \delta^{56}\text{Fe}_A - \delta^{56}\text{Fe}_{\text{Total}} \quad (\text{Eq.2})$$

The internal precisions of the  $\delta^{56}\text{Fe}$  values were calculated for each analytical run using the repeated measurement of the IRMM-014 and SPEX standards and were found to be close to 0.08‰ for  $\delta^{56}\text{Fe}$  (at 2 standard deviation, 2SD). All of the samples were analyzed at least twice, and the mean values of the analyses duplicate are reported with their 95% confidence interval (Supplementary data 1-6, Table S1 to Table S6). The external precision, determined by the duplicated analyses of BHVO-1 was 0.08‰ (2SD, n=12).

## 2.8. Mass balance determination and error propagation

The Fe isotopic composition of each sample (i.e. fraction A) was reported using the average of duplicated analysis. The error propagation of the size fraction A which measured n times, was calculated as:

$$\sigma\delta^{56}\text{Fe}_A = \sqrt{\sum_{i=1}^n \sigma\delta^{56}\text{Fe}_{A_n}^2 / n} \quad (\text{Eq.3})$$

The average of duplicate samples was reported as the Fe isotopic composition of each size fraction and the error propagation was calculated using Eq.3.

The Fe isotopic composition of the size fraction  $F_n$  ( $\delta^{56}\text{Fe}_{F_n}$ ), is calculated based on a mass balance taking into account the  $\delta^{56}\text{Fe}$  and Fe concentrations in the fractions as follows:

$$\delta^{56}\text{Fe}_{F_n} = \sum_{i=1}^n X_{F_i} \delta^{56}\text{Fe}_{F_i} \quad (\text{Eq.4})$$

Where,  $X_{F_i}$  is the Fe concentration of the  $F_i$  fraction. For example, A and B are two size fractions so:

$$\delta^{56}\text{Fe}_{A-B} = (X_A \delta^{56}\text{Fe}_A - X_B \delta^{56}\text{Fe}_B) / X_{A-B} \quad (\text{Eq.5})$$

The Fe isotopic composition and error propagations were calculated using a Monte Carlo simulation (Rouxel *et al.*, 2016) for the calculated size fractions (i.e. > 0.2  $\mu\text{m}$ , 0.2  $\mu\text{m}$ - 30 kDa and 30-5 kDa fractions).

In addition, the Fe isotopic fractionation between two components (i.e. A and B) is expressed as the difference between the  $\delta^{56}\text{Fe}$  values of each component as follows:

$$\Delta^{56}\text{Fe}_{A-B} = \delta^{56}\text{Fe}_A - \delta^{56}\text{Fe}_B \quad (\text{Eq.6})$$

The error propagation of isotope fractionation ( $\sigma \Delta^{56}\text{Fe}_{A-B}$ ) between fraction A and fraction B,  $\sigma (\Delta^{56}\text{Fe}_{A-B})$ , is calculated as:

$$\sigma \Delta^{56}\text{Fe}_{A-B} = \sqrt{(\sigma \delta^{56}\text{Fe}_A)^2 + (\sigma \delta^{56}\text{Fe}_B)^2} \quad (\text{Eq.7})$$

Also the error propagation of the corrected Fe isotope composition ( $\delta^{56}\text{Fe}'$ , Eq.2) is calculated as:

$$\sigma \delta^{56}\text{Fe}' = \sqrt{(\sigma \delta^{56}\text{Fe}_A)^2 + (\sigma \delta^{56}\text{Fe}_{Total})^2} \quad (\text{Eq.8})$$

## 2.9. Speciation modeling

The Fe speciation in the experiments was modeled using PHREEQC-Model VI (Marsac *et al.*, 2011). This model assumes that the complexation of ions by humic substances occurs through eight discrete sites: four weak sites (carboxylic groups) and four strong sites (phenolic groups). The “minteq.v4” database was implemented with the specific binding parameters of Model VI corresponding to the complexation of Fe(II) and Fe(III) with organic matter (Marsac *et al.*, 2013; Catrouillet *et al.*, 2014). The speciation was calculated in conditions allowing the precipitation of ferrihydrite.

## 3. RESULTS

### 3.1. Fe-OM binding experiments

#### 3.1.1. OM-free experiment

In the OM-free experiment at pH 1, 4.9% in the > 0.2  $\mu\text{m}$  fraction as precipitates (oxides and/or hydroxides) and more than 93% of the total Fe was in the < 30 kDa fraction as soluble species (Fig. 1a, Table 1). At pH 2, 7.9% of Fe is precipitated in the > 0.2  $\mu\text{m}$  fraction and 84 % of Fe occurred in the < 30 kDa fraction. PHREEQC-Model VI calculated that, at pH 1 and pH 2, 99.9% and 93% of Fe was as free  $\text{Fe}^{3+}$  species and 0.1% and 6.6% as  $\text{Fe}(\text{OH})_n^{3-n}$ , respectively (Table 2). At pH 6.5, 65% of Fe occurred in the > 0.2  $\mu\text{m}$  fraction and < 0.1% of Fe was in the < 30 kDa fraction (Table 1). PHREEQC-Model VI predicted that 100% of Fe was precipitated as ferrihydrite (Table 2).

At pH 1,  $\delta^{56}\text{Fe}$  ranged from  $0.50 \pm 0.05\text{‰}$  ( $2\sigma$ ) to  $0.57 \pm 0.05\text{‰}$  ( $2\sigma$ ) (Fig. 1b, Table 1) for all measured fractions (i.e. total, < 0.2  $\mu\text{m}$ , < 30 kDa, < 5 kDa), yielding  $\delta^{56}\text{Fe}'$  close to 0‰. Therefore, no significant Fe isotope fractionation was observed by filtration and ultrafiltration, which is consistent with mass balance considerations since Fe was quantitatively transferred through the filtration membranes regardless of pore sizes. As a consequence, the negligible amount of Fe calculated for the > 0.2  $\mu\text{m}$ , 0.2  $\mu\text{m}$  - 30 kDa and 30 kDa-5 kDa fractions precludes a robust determination of their Fe isotope signatures (Supplementary data 7, Table S7).

At pH 2,  $\delta^{56}\text{Fe}$  ranged from  $0.61 \pm 0.03\text{‰}$  for the total fraction to  $0.83 \pm 0.03\text{‰}$  for the < 5 kDa fraction, yielding  $\delta^{56}\text{Fe}' = 0.22 \pm 0.04\text{‰}$  for < 5 kDa,  $0.14 \pm 0.04\text{‰}$  for < 30 kDa and  $0.08 \pm 0.04\text{‰}$  for < 0.2  $\mu\text{m}$  (Table 1). Mass balance determination (Eq.5) showed significant Fe isotope fractionations between the > 0.2  $\mu\text{m}$  and < 5 kDa Fe, and between the 0.2  $\mu\text{m}$  - 30 kDa and < 5 kDa pools at  $-1.16 \pm 0.66\text{‰}$  and  $-0.80 \pm 0.50\text{‰}$ , respectively (Table 3).

At pH 6.5,  $\delta^{56}\text{Fe}$  of the < 0.2  $\mu\text{m}$  fraction was identical, within uncertainty, to that of the total fraction ( $0.55 \pm 0.05\text{‰}$  and  $0.61 \pm 0.05\text{‰}$ , respectively) despite retention of approximately 65% of Fe in the > 0.2  $\mu\text{m}$  fraction. This yields  $\delta^{56}\text{Fe}'$  values for < 0.2  $\mu\text{m}$  and > 0.2  $\mu\text{m}$  near 0 ‰ suggesting a lack of Fe isotope fractionation under these experimental conditions. Isotopic analysis of the < 30 kDa and < 5 kDa fractions could not be performed due to too low Fe concentrations ( $[\text{Fe}] < 40 \text{ nmol L}^{-1}$ ). Hence, under these experimental conditions, dissolved Fe occurs essentially in the 0.2  $\mu\text{m}$ -30 kDa fraction.

### 3.1.2. Fe-free experiment

The Fe-free experiments were performed at pH 2 and pH 6.5. At pH 2, 56% of OM was in the  $> 0.2 \mu\text{m}$  fraction, compared to 20% at pH 6.5 (Fig. 2, Table 4). Approximately 32% of OM was in the  $< 30 \text{ kDa}$  fraction, whereas these proportions increased to 42% at pH 6.5. The initial Fe content of OM was  $8.3 \pm 0.13 \mu\text{mol L}^{-1}$ , but Fe remained undetected in the  $< 0.2 \mu\text{m}$  fractions. The amount of initial Fe content of OM corresponds to about 9 % of total Fe loading for all other experiments with Fe and OM. Considering a mean of  $\delta^{56}\text{Fe} = 0.09 \pm 0.03\text{‰}$  for the initial OM, the maximum effect of Fe impurities on  $\delta^{56}\text{Fe}$  of total Fe represent only 0.06 ‰, which is close to the analytical uncertainty. Regardless of this effect, no specific correction was needed for Fe-OM binding experiment.

### 3.1.3. Fe-OM binding experiment

At pH 1, 97% of Fe occurred in the  $< 0.2 \mu\text{m}$  fraction (Fig. 3a, Table 5) whereas only 24% of OM was recovered in the same fraction. The high retention of OM, 76%, in the  $> 0.2 \mu\text{m}$  fraction resulted from flocculation/precipitation reactions (Fig. 3b). Similar features were observed for the  $< 30 \text{ kDa}$  and  $< 5 \text{ kDa}$  fractions (i.e. similar to OM-free experiments), e.g. about 90% of total Fe and 22% of OM were recovered in  $< 5 \text{ kDa}$  fraction.

At pH 2, 51% of Fe and 9.9% of OM were recovered in the  $< 0.2 \mu\text{m}$  fraction, and 48% of Fe and 8.6% of OM were in the  $< 30 \text{ kDa}$  fraction. The percentages of Fe and OM in the  $0.2 \mu\text{m} - 30 \text{ kDa}$  fraction were therefore insignificant. However, the  $> 0.2 \mu\text{m}$  fraction represented 49% of the total Fe suggesting a significant Fe-OM flocculation process at pH 2. At pH 6.5, 43% of Fe and 57% of OM were in the  $< 0.2 \mu\text{m}$  fraction and only 0.8% of Fe and 20% of OM were in the  $< 30 \text{ kDa}$  fraction, indicating that 42% of Fe and 38% of OM occurred in the  $0.2 \mu\text{m} - 30 \text{ kDa}$  fraction. At pH 1, PHREEQC-Model VI predicted that 91% and 8.7% of Fe was as free  $\text{Fe}^{3+}$  and Fe-OM complexes, respectively (Table 2). At pH 2, Fe-OM increased to 31%, whereas  $\text{Fe}^{3+}$  decreased to 64%. At this low pH, no ferrihydrite is expected to precipitate. At pH 1, with or without OM, Fe bound to  $\text{OH}^-$  represented only 0.1% of the total Fe (Table 2). However, at pH 2 with OM, the amount of Fe bound to  $\text{OH}^-$  increased to 4.6%, which is slightly lower than without OM. At pH 6.5, modeling calculations showed that 94% of Fe precipitated as ferrihydrite, whereas 5.7% of Fe occurred as Fe-OM complexes. No  $\text{Fe}(\text{OH})_n^{3-n}$

was expected at this pH (Table 2). The Fe(II) concentration was measured through ferrozine test at pH 1, 2 and 6.5. The results showed that the Fe(II) concentration was below the detection limit ( $< 2.2 \mu\text{mol L}^{-1}$ ) and no Fe(II) was produced during this Fe-OM binding experiment.

Fig. 3c shows the  $\delta^{56}\text{Fe}$  variations in the size fractions at each pH. At pH 1, because of low concentration of Fe in the  $> 0.2 \mu\text{m}$  and  $0.2 \mu\text{m} - 30 \text{ kDa}$  fractions mass balance relationships yielded large uncertainties (Supplementary data 8, Table S8). Therefore, no obvious isotopic variations were observed, which is similar to OM-free experiment. At pH 2, the  $< 0.2 \mu\text{m}$ ,  $< 30 \text{ kDa}$  and  $< 5 \text{ kDa}$  fractions showed clear variations relative to the total Fe fraction, yielding  $\delta^{56}\text{Fe}' = -0.48 \pm 0.06\text{‰}$ ;  $-0.45 \pm 0.06\text{‰}$  and  $-0.44 \pm 0.06\text{‰}$  respectively (Table 5). Mass balance calculation (Eq.5) demonstrated significant Fe isotope fractionations between the  $> 0.2 \mu\text{m}$  and  $30 \text{ kDa} - 5 \text{ kDa}$  with  $\Delta^{56}\text{Fe}_{>0.2 \mu\text{m} - (30 \text{ kDa}-5 \text{ kDa})} = 1.02 \pm 0.64\text{‰}$  and, between the  $> 0.2 \mu\text{m}$  and  $< 5 \text{ kDa}$  fractions at  $0.94 \pm 0.11\text{‰}$  (Table 3). At pH 6.5, an opposite trend was observed, with  $\delta^{56}\text{Fe}' = 0.07 \pm 0.05\text{‰}$  for the  $< 0.2 \mu\text{m}$  fraction, and  $\delta^{56}\text{Fe}' = 0.35 \pm 0.06\text{‰}$  for the  $< 30 \text{ kDa}$  (Fig. 3c). The results suggested significant Fe isotopic fractionations between Fe pools, yielding  $\Delta^{56}\text{Fe}_{>0.2 \mu\text{m} - (0.2 \mu\text{m}-30 \text{ kDa})} = -0.11 \pm 0.08\text{‰}$ ;  $\Delta^{56}\text{Fe}_{>0.2 \mu\text{m} - <30 \text{ kDa}} = -0.40 \pm 0.08\text{‰}$  and  $\Delta^{56}\text{Fe}_{(0.2 \mu\text{m}-30 \text{ kDa}) - <30 \text{ kDa}} = -0.29 \pm 0.05\text{‰}$  (Table 3).

### 3.2. Experiments of organic matter titration by Fe

In the Fe-OM titration experiment at pH 2, 16% of Fe and 80% of OM were in the  $> 0.2 \mu\text{m}$  fraction as precipitated and/or flocculated species (Fig. 4 and Table 6). In contrast to binding experiment, the  $30 \text{ kDa} - 5 \text{ kDa}$  fraction represented a very small pool of total Fe. However the  $0.2 \mu\text{m} - 30 \text{ kDa}$  fraction represented a larger Fe pool compared to the binding experiment at similar pH. About 76% of Fe and 19% of OM were recovered in both the  $< 30 \text{ kDa}$  and  $< 5 \text{ kDa}$  fractions. Iron therefore mainly occurred in the smaller fractions. At pH 6.5, 41% of Fe and 31% of OM occurred in the  $> 0.2 \mu\text{m}$  fraction (Table 6), which is substantially higher than pH 2 experiment but significantly lower than Fe-OM binding experiments at the same pH (Table 5). The  $< 30 \text{ kDa}$  fraction contained the remaining 3.5% of Fe and 19% of OM. Therefore, 56% of Fe and 50% of OM were in the  $0.2 \mu\text{m} - 30 \text{ kDa}$  fraction.

At pH 2, the  $< 0.2 \mu\text{m}$ ,  $< 30 \text{ kDa}$  and  $< 5 \text{ kDa}$  fractions are enriched in light Fe isotopes relative to the total Fe, yielding  $\delta^{56}\text{Fe}'_{<0.2 \mu\text{m}} = -0.49 \pm 0.06\text{‰}$  and  $\delta^{56}\text{Fe}'_{<30 \text{ kDa}} = -0.48 \pm$

0.06‰, with similar value for < 5 kDa fraction (Fig. 4c and Table 6). These results are remarkably similar to those obtained for the Fe-OM the binding experiment at pH 2. The Fe isotope fractionation factor between the > 0.2  $\mu\text{m}$  and 0.2  $\mu\text{m}$  -30 kDa was determined at  $2.78 \pm 0.91\text{‰}$  (Table 3). Similar values were also obtained for the Fe-OM the binding experiment at the same pH, with  $\Delta^{56}\text{Fe}_{>0.2\ \mu\text{m} - <5\ \text{kDa}} = 3.02 \pm 0.62\text{‰}$  (Table 3). In contrast to binding experiment, Fe isotopic fractionation was not significant between the > 0.2  $\mu\text{m}$  and 30 kDa -5 kDa fractions, because of low Fe concentration in the 30 kDa -5 kDa fraction. At pH 6.5, the < 30 kDa fraction ( $\delta^{56}\text{Fe}_{<30\ \text{kDa}} = 0.80 \pm 0.03\text{‰}$ ) displayed a heavier Fe isotope composition than the total fraction ( $\delta^{56}\text{Fe}_{\text{total}} = 0.54 \pm 0.04\text{‰}$ ), yielding a  $\delta^{56}\text{Fe}'_{<30\ \text{kDa}} = 0.26 \pm 0.05\text{‰}$  (Fig. 4c, Table 6). This result is also comparable to that of the Fe-OM binding experiment at the same pH and opposite to the results obtained at pH 2. Mass balance (Eq.5) determined the Fe fractionation factor between the > 0.2  $\mu\text{m}$  and < 30 kDa at  $-0.32 \pm 0.11\text{‰}$  and also between the 0.2  $\mu\text{m}$  -30 kDa and < 30 kDa at  $-0.23 \pm 0.05\text{‰}$  (Table 3 and Supplementary data 9, Table S9). No significant Fe isotope fractionation was observed within uncertainty between the > 0.2  $\mu\text{m}$  and 0.2  $\mu\text{m}$  -30 kDa fractions.

### 3.3. Organic matter deposition experiment

At pH 2, 55% of Fe and 69% of OM were retained in the > 0.2  $\mu\text{m}$  fraction (Fig. 5 and Table 7). Hence, a higher proportion of Fe was retained in the > 0.2  $\mu\text{m}$  fraction compared to the Fe-OM binding and titration experiments (49% and 16% of Fe in the Fe-OM binding and titration experiments, respectively). The < 30 kDa fraction contained 14% of Fe and 8% of OM. Hence, mass balance considerations (Eq.5) showed that the 0.2  $\mu\text{m}$  - 30 kDa fraction contained about 31% of Fe and 23% of OM. At pH 6.5, 89% of Fe and 23% of OM retained in the > 0.2  $\mu\text{m}$  fraction. Although less OM was retained as compared to pH 2, the amount of retained Fe was higher, as shown by a  $\text{Fe}/\text{C}_{\text{org}}$  (mol./mol.) ratio of 0.004 at pH 2 against 0.017 at pH 6.5. Iron in the < 0.2  $\mu\text{m}$  fraction represented approximately 11% of the total Fe. The < 30 and < 5 kDa fractions contained undetectable Fe and 16% and 7% of OM respectively (Fig. 5 and Table 7).

At pH 2, the < 5 kDa fraction was characterized by significant enrichment in light Fe isotopes relative to the total Fe ( $\delta^{56}\text{Fe}'_{<5\ \text{kDa}} = -0.23 \pm 0.06\text{‰}$ ) (Table 7) while the < 30 kDa yielded similar composition that the total Fe. Hence, unlike the other experiments, significant Fe fractionations were observed between the > 0.2  $\mu\text{m}$  and 30 kDa- 5 kDa fractions

( $\Delta^{56}\text{Fe}_{>0.2\ \mu\text{m} - (30\ \text{kDa} - 5\ \text{kDa})} = -3.12 \pm 1.34\text{‰}$ ), the  $> 0.2\ \mu\text{m}$  and  $< 5\ \text{kDa}$  fractions ( $\Delta^{56}\text{Fe}_{>0.2\ \mu\text{m} - <5\ \text{kDa}} = 0.21 \pm 0.09\text{‰}$ ), the  $0.2\ \mu\text{m}$ - $30\ \text{kDa}$  and  $30\ \text{kDa}$ - $5\ \text{kDa}$  fractions ( $\Delta^{56}\text{Fe}_{(0.2\ \mu\text{m} - 30\ \text{kDa}) - (30\ \text{kDa} - 5\ \text{kDa})} = -3.09 \pm 1.34\text{‰}$ ), the  $0.2\ \mu\text{m}$ - $30\ \text{kDa}$  and  $< 5\ \text{kDa}$  fractions ( $\Delta^{56}\text{Fe}_{(0.2\ \mu\text{m} - 30\ \text{kDa}) - <5\ \text{kDa}} = 0.24 \pm 0.07\text{‰}$ ) and the  $30\ \text{kDa}$ - $5\ \text{kDa}$  and  $< 5\ \text{kDa}$  fractions ( $\Delta^{56}\text{Fe}_{(30\ \text{kDa} - 5\ \text{kDa}) - <5\ \text{kDa}} = 3.33 \pm 1.34\text{‰}$ )(Table 3).

At pH 6.5, the  $< 0.2\ \mu\text{m}$  fraction was enriched in light Fe isotope compared to the total fraction, with  $\delta^{56}\text{Fe}'_{<0.2\ \mu\text{m}} = -0.35 \pm 0.06\text{‰}$  (Table 7). Since Fe concentrations were too low (i.e. below detection), the  $\delta^{56}\text{Fe}$  could not be determined in the  $< 30\ \text{kDa}$  and  $< 5\ \text{kDa}$  fractions. Mass balance (Eq.5) resulted a Fe isotope fractionation between the  $> 0.2\ \mu\text{m}$  and  $< 0.2\ \mu\text{m}$  fractions for  $0.39 \pm 0.06\text{‰}$  (Table 3).

### 3.4. Natural Fe-OM associations

In the natural Fe-OM associations, 12% of Fe and 10% of OM were found in the  $> 5\ \mu\text{m}$  particulate fraction, while 47% of Fe and 24% of OM were retained in the  $5\ \mu\text{m}$  -  $0.2\ \mu\text{m}$  fraction (Fig. 6 and Table 8). The  $0.2\ \mu\text{m}$  -  $30\ \text{kDa}$  fraction contained 35% of Fe and 32% of OM. The remaining Fe (7%) and OM (34%) were in the  $< 30\ \text{kDa}$  fraction (Fig. 6 and Table 8).

The total fraction was characterized by a  $\delta^{56}\text{Fe}$  of  $0.17 \pm 0.03\text{‰}$ , which represented the composition of the initial soil solution. In contrast, the  $> 5\ \mu\text{m}$  fraction displayed heavier Fe isotope composition with  $\delta^{56}\text{Fe} = 0.32 \pm 0.04\text{‰}$  (Fig. 6c and Table 8). Using a mass balance approach (Eq.5) demonstrated that the  $0.2\ \mu\text{m}$  -  $30\ \text{kDa}$  fraction ( $\delta^{56}\text{Fe} = 0.06 \pm 0.03\text{‰}$ ) was characterized by significant enrichment in light isotopes relative to the  $5\ \mu\text{m}$  -  $0.2\ \mu\text{m}$  fraction ( $\delta^{56}\text{Fe} = 0.16 \pm 0.03\text{‰}$ ). The Fe isotopic compositions of the  $< 30\ \text{kDa}$  and  $< 5\ \text{kDa}$  fractions were similar within uncertainty, and ranged from  $\delta^{56}\text{Fe} = 0.34 \pm 0.03\text{‰}$  to  $0.40 \pm 0.07\text{‰}$ . They were thus enriched in heavy Fe isotopes relative the total fraction for  $\delta^{56}\text{Fe}' = 0.17 \pm 0.04\text{‰}$  and  $0.23 \pm 0.08\text{‰}$ , respectively (Table 8). The  $< 5\ \text{kDa}$  fraction was therefore enriched in heavy Fe isotopes relative to the other fractions. In contrast to these isotopically heavy fraction, the  $0.2\ \mu\text{m}$  -  $30\ \text{kDa}$  fraction was enriched in lighter Fe isotopes with  $\delta^{56}\text{Fe} = 0.06 \pm 0.03\text{‰}$ . Significant Fe isotope fractionations were observed between the  $> 5\ \mu\text{m}$  fraction and other fraction with  $\Delta^{56}\text{Fe}_{>5\ \mu\text{m} - (5\ \mu\text{m} - 0.2\ \mu\text{m})} = 0.16 \pm 0.05\text{‰}$ ,  $\Delta^{56}\text{Fe}_{>5\ \mu\text{m} - (0.2\ \mu\text{m} - 30\ \text{kDa})} = 0.26 \pm 0.04\text{‰}$  and  $\Delta^{56}\text{Fe}_{>5\ \mu\text{m} - (30\ \text{kDa} - 5\ \text{kDa})} = 0.21 \pm 0.09\text{‰}$  (Table 3). The smallest  $< 5\ \text{kDa}$  fraction presented the highest  $\delta^{56}\text{Fe}$ . These Fe isotope fractionations were observed be-

tween the 5  $\mu\text{m}$  - 0.2  $\mu\text{m}$  and the < 5 kDa fractions ( $\Delta^{56}\text{Fe}_{(5 \mu\text{m} - 0.2 \mu\text{m}) - < 5\text{kDa}} = -0.24 \pm 0.08\text{‰}$ ) and the 0.2  $\mu\text{m}$  - 30 kDa, and the < 5 kDa fractions ( $\Delta^{56}\text{Fe}_{(0.2 \mu\text{m} - 30 \text{kDa}) - < 5\text{kDa}} = -0.33 \pm 0.08\text{‰}$ ).

## 4. DISCUSSION

### 4.1. Impact of precipitation on Fe isotopic fractionation

In the OM-free experiment, precipitation was shown to occur mainly at pH 2 and 6.5. At pH 6.5 and as predicted by the PHREEQC-Model VI (Table 2), Fe occurred mainly as Fe-oxyhydroxides in the > 0.2  $\mu\text{m}$  fraction. The low Fe concentrations in the < 5 kDa and < 30 kDa fractions precluded the determination of Fe isotopic composition of these fractions. Moreover, the calculation of the Fe isotopic fractionation factor between the > 0.2  $\mu\text{m}$  and the < 0.2  $\mu\text{m}$  fractions was insignificant, with  $\Delta^{56}\text{Fe}_{> 0.2 \mu\text{m} - < 0.2 \mu\text{m}} = 0.09 \pm 0.10\text{‰}$  (Table 1), suggesting that Fe precipitation as ferrihydrite did not produce any Fe isotope fractionation. In contrast, at pH 2, the major pool of Fe was in the < 5 kDa fraction (about 80%) in which, Fe occurred as free or soluble complexes in agreement with modeling results (Table 2). The resulting Fe isotopic fractionation between the > 0.2  $\mu\text{m}$  and the < 5 kDa fractions was significant, with  $\Delta^{56}\text{Fe}_{> 0.2 \mu\text{m} - < 5 \text{kDa}} = -1.16 \pm 0.66 \text{‰}$ . Note that this value is also similar to  $\Delta^{56}\text{Fe}_{> 5 \text{kDa} - < 5 \text{kDa}}$  and has relatively high propagated uncertainties due to the small pool of Fe retained on the membrane > 0.2  $\mu\text{m}$ . Nevertheless, the <5 kDa fraction appears systematically enriched in heavy Fe isotopes relative to both > 0.2  $\mu\text{m}$  and 0.2  $\mu\text{m}$ -30 kDa fractions. An immediate implication of this result is that kinetic or diffusion effects during ultrafiltration were likely minor or insignificant (i.e. a light Fe isotope enrichment would be expected for the fraction passing through the membrane). As discussed by *Roe et al. (2003)*, Fe-OH binding favors the complexation of heavy relative to light Fe isotopes. In addition, as mentioned in previous section, according to modeling, about 6.6% of the total Fe is present as soluble  $\text{Fe}(\text{OH})_n^{3-n}$  complexes in the < 5 kDa fraction. At pH 2, the Fe isotope fractionation factor between the > 0.2  $\mu\text{m}$  and the < 5 kDa fractions could therefore result from the small amount of Fe complexed by  $\text{OH}^-$  ligands. These results also provided evidence that Fe precipitation has no direct impact on the Fe isotopes fractionation. *Skulan et al. (2002)* demonstrated also that no Fe isotopic fractionation occurred between  $\text{Fe}^{3+}$  and hematite ( $\Delta^{56}\text{Fe}_{\text{Fe}^{3+} - \text{hematite}} = -0.10 \pm 0.20\text{‰}$ ) at low and high (98°C) temperatures.

#### 4.2. Impact of OM on Fe isotopic fractionation

In the Fe-OM binding experiment, at pH 1, Fe occurred mainly in the < 30 kDa fraction as free Fe<sup>3+</sup> has identical Fe isotope composition, within uncertainty, than the total Fe. Considering that the < 30 kDa fraction represented about 92% of the total Fe, determining the Fe isotope composition of the > 0.2 μm and 0.2 μm - 30 kDa fractions through mass balance relationships yielded large uncertainties, preventing the determination of Fe isotope fractionation factor during filtration. Regardless the pH, high OM proportions in the > 0.2 μm fraction suggested that Fe promoted OM coagulation or flocculation (e.g. at pH 2, 90% versus 56% of OM in the > 0.2 μm fraction with and without Fe, respectively). At pH 2, the higher proportion of Fe and OM in the > 0.2 μm fraction indicated that Fe precipitated as a mixture of OM and Fe-oxyhydroxide particles. However, a large amount of Fe was also present in the < 30 kDa fraction as free Fe<sup>3+</sup>. Moreover, at pH 2, complexation and precipitation occurred simultaneously. At this pH, all the < 0.2 μm fractions consistently showed an enrichment in Fe light isotopes relative to the total fraction. Mass balance considerations and error propagation (Eq.5) yielded  $\delta^{56}\text{Fe}_{>0.2\ \mu\text{m}} = 1.02 \pm 0.10\text{‰}$  (Table 5) and  $\Delta^{56}\text{Fe}_{>0.2\ \mu\text{m} - <0.2\ \mu\text{m}} = 0.97 \pm 0.11\ \text{‰}$  (Table 3). Modeling calculations demonstrated that 31% of the Fe was bound to OM, whereas roughly 4.6% occurred as Fe(OH)<sub>n</sub><sup>3-n</sup> (Table 2). Several authors showed that the strong Fe-O bonds are formed via the O atoms of the OM carboxylic sites in bidentate or tridentate complexes (Catrouillet *et al.*, 2014) between heavy Fe isotopes and OM (Dideriksen *et al.*, 2008; Morgan *et al.*, 2010). At pH 2, Fe was partially complexed by OM, which is precipitated at this low pH. Iron was thus associated to large organic precipitates whose size was > 0.2 μm. Due to the preferential complexation of heavy Fe isotopes by OM, flocculation processes and OM precipitation is expected to produce isotopically light Fe in the remaining < 0.2 μm fraction. At pH 6.5, in the < 30 kDa fraction, Fe concentration was low and OM represented only 19.7% of the total OM. These results provided evidence of the simultaneous Fe and OM precipitation in the highest fractions. According to the model (Table 2), 5.7% of Fe were complexed by OM, suggesting that all of the Fe present in the < 30 kDa fraction could be bound to OM. Thereby, the observed Fe isotopic fractionation between the > 0.2 μm and the < 30 kDa fractions ( $\Delta^{56}\text{Fe}_{>0.2\ \mu\text{m} - <30\ \text{kDa}} = -0.40 \pm 0.08\text{‰}$ ) can be explained by the Fe-OM complexes as discussed above. The present results thus showed that Fe complexation by OM and OH<sup>-</sup> may drive significant and negative Fe isotopic fraction-

ation factor between  $> 0.2 \mu\text{m}$  and  $< 30 \text{ kDa}$ . As calculated by PHREEQC-Model VI, Fe-OM complexation is dominant at pH 6.5 (Table 2), leading to a negative  $\Delta^{56}\text{Fe}_{>0.2\mu\text{m} - <30 \text{ kDa}}$  ( $-0.40 \pm 0.08\text{‰}$  and  $-0.32 \pm 0.11\text{‰}$  in the binding and titration experiments, respectively). Equilibrium Fe isotope fractionation due to organic ligand exchange was studied by *Morgan et al. 2010*. These authors displayed that despite the strong binding affinity of siderophore ligands (e.g. desferrioxamine mesylate) for Fe, Fe isotopes exchange between siderophore ligands and ligands with lower Fe-binding affinities. They also suggested a positive correlation between Fe-ligand binding affinity and the magnitude of equilibrium isotope fractionation. Our findings are consistent with their results to support the hypothesis of Fe isotope fractionation resulting from Fe-binding to organic ligands with high affinities.

Unexpected results (i.e. strong isotope fractionation) were however obtained at pH 2 where OM complexation was not expected to be dominant. Calculated fractionation factors between the  $> 0.2 \mu\text{m}$  and  $< 0.2 \mu\text{m}$  Fe pools were determined at  $0.97 \pm 0.11\text{‰}$  and  $3.04 \pm 0.62\text{‰}$ , for the binding and titration experiments, respectively. As described by *Allard et al. (2004)* at  $\text{pH} < 5$ , precipitation competed with Fe complexation due to the lower solubility of Fe in the presence of OM. PHREEQC-Model VI calculated that 69% of Fe occurred as dissolved species ( $\text{Fe}^{3+}$  and  $\text{Fe}(\text{OH})_n^{3-n}$ ) at pH 2 in the presence of OM and reached 100% in the OM-free experiment (Table 2). Therefore, at pH 2, Fe binding by OM was rather inefficient compared to Fe precipitation as aggregates. Therefore, we interpret the rather large Fe fractionation factor  $\Delta^{56}\text{Fe}_{>0.2 \mu\text{m} - <0.2 \mu\text{m}}$  as resulting from the preferential binding of heavy Fe isotopes by OM in the particulate fraction, yielding a decrease in the  $\delta^{56}\text{Fe}$  in the dissolved Fe fractions.

The Fe-organic ligand complexation was reported as a potential cause of Fe isotope fractionation in natural environment in several studies. In particular, *Conway and John, (2014)* and *Fitzsimmons et al. (2015)* suggested that the strong Fe-binding ligands could be due to concentration of heavy Fe isotopes and the Fe isotope enrichment in the range from 0.3 to 0.7 ‰ in seawater. Natural environments waters such as stream characterized by an enrichment in heavy Fe isotopes in the  $< 0.2 \mu\text{m}$  fractions, Fe complexation by OM may be the dominant process controlling the Fe isotopic composition (i.e. 2 ‰, *Ilina et al., 2013*). The organic molecules as siderophores or macromolecules can precipitate and form flocs larger than  $0.2 \mu\text{m}$ , notably at low pH. Therefore, under physico-chemical conditions where Fe complexation by OM and flocculation are favored, OM-rich fractions are enriched in

heavy Fe isotopes. The similar result was reported by *Fitzsimmons et al. 2016*, presenting the complexation Fe-organic ligand as a reason of colloidal phase enrichment in heavy Fe isotopes for  $\delta^{56}\text{Fe} = 0.54 \pm 0.14\text{‰}$  in a hydrothermal plume study.

#### 4.3. Impact of filtration and ultrafiltration on Fe isotopic fractionation

The OM-free experiment provided a first-order assessment of the fractionation of Fe isotopes during (ultra)filtration. At pH 1, Fe was mainly present as soluble species in the  $< 0.2 \mu\text{m}$ ,  $< 30 \text{ kDa}$  and  $< 5 \text{ kDa}$  fractions and no Fe isotope fractionation could be expressed. The pore size modification was mentioned as a usual problem of (ultra)filtration. Previously *Illina et al. (2013)* demonstrated that (ultra)filtration cannot fractionate the Fe isotopes through a procedure check using non-cascade mode filtration. The OM deposition experiment was specially designed to test this hypothesis. At pH 2, OM and Fe were mainly retained in the  $> 0.2 \mu\text{m}$  fraction in response to the combination of the OM precipitation and the possible Fe binding with OM. The modeling calculation showed indeed that 31% of Fe was complexed to OM (Table 2). The Fe isotopic composition of the  $< 5 \text{ kDa}$  fraction,  $\delta^{56}\text{Fe}'_{< 5 \text{ kDa}} = -0.23 \pm 0.06\text{‰}$  (Table 7) suggested a significant enrichment in light isotopes in this fraction. However, this enrichment in light Fe isotopes at the  $< 5 \text{ kDa}$  was not observed when Fe and OM were simultaneously (ultra)filtered in the binding experiment at pH 2. In the binding experiment, Fe was bound to OM before the (ultra)filtration and then the equilibrium was reached between different fractions. In such conditions, the presence of relatively high concentration of Fe promoted OM molecules flocculation, which resulted in aggregates having higher Fe/OM. However, in the OM deposition experiment, the acidic pH was the only parameter able to precipitate OM molecules, which results in the formation of smaller-size organic-rich colloids that were recovered in the  $> 5 \text{ kDa}$  fraction. During the Fe filtration, Fe was partially bound to these small deposited organic colloids. The Fe isotopic fractionation between the  $> 5 \text{ kDa}$  and the  $< 5 \text{ kDa}$  fractions was positive with  $\Delta^{56}\text{Fe}_{> 5 \text{ kDa} - < 5 \text{ kDa}} = 0.26 \pm 0.05\text{‰}$ . Therefore, the binding of isotopically heavy Fe with OM deposited on the 5 kDa membrane led to an enrichment of the  $< 5 \text{ kDa}$  fraction in light Fe isotopes. Iron isotopic fractionation in the  $< 5 \text{ kDa}$  fraction results therefore from the Fe binding to small organic molecules deposited on the membrane.

At pH 6.5, a higher Fe amount occurred in the  $> 0.2 \mu\text{m}$  fraction as compared to the experiment without OM in response to the Fe precipitation. Lighter Fe isotopic composition was

measured in the  $< 0.2 \mu\text{m}$  fraction ( $\delta^{56}\text{Fe}'_{< 0.2 \mu\text{m}} = -0.35 \pm 0.06\text{‰}$ ). In the OM deposition experiment, Fe was bound to OM and/or precipitated as ferrihydrite. The consequence was an enrichment in light Fe isotopes and low concentration of Fe in the  $< 0.2 \mu\text{m}$  fraction induced by their complexation with the OM deposited on the  $> 0.2 \mu\text{m}$  membrane. The OM deposition experimental conditions favored the Fe binding with OM that coated the filtration membrane and subsequently the fractionation of the Fe isotopes. The observed Fe fractionation obtained in the OM deposition experiment was therefore not produced directly by the (ultra)filtration technique.

#### 4.4. Mechanisms controlling Fe fractionation

The  $\delta^{56}\text{Fe}$  measured for all of the fractions from the OM-free, binding, titration and deposition experiments at pH 6.5 were plotted relative to the Fe concentration (Fig. 7). The majority of the fractions exhibited an isotopic composition  $\delta^{56}\text{Fe}$  in the range from  $0.48 \pm 0.03\text{‰}$  to  $0.61 \pm 0.05\text{‰}$ . The two highest  $\delta^{56}\text{Fe}$  values reached  $0.83 \pm 0.03\text{‰}$  and  $0.80 \pm 0.03\text{‰}$  and corresponded to the  $< 30 \text{ kDa}$  fractions where Fe was expected to be bound to small OM molecules. The lowest  $\delta^{56}\text{Fe}$  ( $0.18 \pm 0.04\text{‰}$ ) corresponded to the  $< 0.2 \mu\text{m}$  fraction in the deposition experiment, in response to flocculation of complexed Fe-OM. However, it is important to note that in the deposition experiment, complexation occurred directly on the OM-coated membrane at  $0.2 \mu\text{m}$  involving heavy Fe isotope retention and their subsequent depletion in the  $< 0.2 \mu\text{m}$  fraction.

All of these experimental results provided evidence that Fe precipitation alone (i.e. in the absence of OM-complexes) was not able to fractionate Fe isotopes. Likewise, the experiments demonstrated that Fe-OM complexation involved Fe fractionation and that this isotopic fractionation increased with increasing pH. The OM deposition on the (ultra)filtration membrane indirectly fractionated Fe isotopes in response to Fe complexation by the trapped OM. However, this process is probably insignificant in natural waters, given that, under natural conditions, Fe is bound to OM before the filtration is performed, i.e. Fe fractionation is produced before (ultra)filtration.

#### 4.5. Application to “natural” Fe-OM associations

Iron-OM associations produced from the oxidation of a reduced soil solution were extensively characterized using X-ray absorption spectroscopy (XAS), transmission electronic microscopy (MET), fluorescence spectral analysis (EEM) and THM-Gas chromatography-mass spectrometry (THM-GC-MS) in a previous study (Guénet *et al.*, 2017). In summary, the particulate fraction ( $> 0.2 \mu\text{m}$ ) was composed of fresh biological OM containing fragments and leaf debris mixed with humic acids (increasing from the  $> 5 \mu\text{m}$  fraction to the  $> 0.2 \mu\text{m}$  fraction). Iron was found as old inherited Fe(III) oxyhydroxides (goethite) or as nano-particles of hydrous Fe(III) oxides embedded within the OM matrix (Fig. 8a and 8b). Approximately 47% of the total Fe occurred in the particulate fraction  $5 \mu\text{m} - 0.2 \mu\text{m}$ . In the colloidal  $0.2 \mu\text{m} - 30 \text{kDa}$  fraction, OM occurred as aggregates of humic substances embedding Fe(III) nano-particles and clusters (Fig. 8c). In the  $< 30 \text{kDa}$  fraction, OM was found as small humic molecules binding to Fe(III) as small clusters or ions. This fraction represented less than 7% of the total Fe. Note that in this experiment, Fe oxidation may be produced by both biotic and abiotic reactions.

The  $\delta^{56}\text{Fe}$  of the reoxidized soil suspension (i.e. the total fraction) was  $0.17 \pm 0.03\text{‰}$ . The highest  $\delta^{56}\text{Fe}$  were obtained in the  $< 30 \text{kDa}$  fraction ( $\delta^{56}\text{Fe}_{< 30 \text{kDa}} = 0.34 \pm 0.03\text{‰}$  with 7% of Fe) and the  $< 5 \text{kDa}$  fraction ( $\delta^{56}\text{Fe}_{< 5 \text{kDa}} = 0.40 \pm 0.07\text{‰}$  with 0.5% of Fe), respectively (Fig. 9 and Table 8). The lowest  $\delta^{56}\text{Fe}$  value was obtained for the  $0.2 \mu\text{m} - 30 \text{kDa}$  fraction ( $\delta^{56}\text{Fe}_{(0.2 \mu\text{m} - 30 \text{kDa})} = 0.06 \pm 0.03\text{‰}$  with 35% of Fe). The  $\delta^{56}\text{Fe}$  increased with the decreasing Fe and DOC concentrations, except for the  $0.2 \mu\text{m} - 30 \text{kDa}$  fraction, without any significant dependence on the pore size (Fig. 9). A similar relationship was also observed by Iliina *et al.*, (2013). These authors reported that the  $\delta^{57}\text{Fe}$  increase with the decreasing Fe/C ratio and the size fraction, which can be due to the changes in chemical nature of Fe-binding from Fe-O-Fe in the large Fe-rich size fractions to Fe-O-C in the small Fe-poor fractions. However, our results displayed that the Fe isotopic signature was controlled not only by the Fe concentration but also the OM played an essential role to control the  $\delta^{56}\text{Fe}$  by the Fe-OM complexation.

The alone Fe cannot explain the  $\delta^{56}\text{Fe}$  in each fraction. Our experimental results provided evidence that Fe complexation with OM produced a significant Fe isotope fractionation and resulted in a negative  $\Delta^{56}\text{Fe}$  between the larger fractions ( $> 30 \text{kDa}$ ) and the small fractions ( $< 5 \text{kDa}$ ). Here, fraction characterization through transmission electron microscopy demonstrated that the  $< 5 \text{kDa}$  fraction primarily contained dissolved Fe(III) monomers or

clusters complexed with OM (Fig.8). Mass balance (Eq.5) and error propagation calculation showed a high and negative  $\Delta^{56}\text{Fe}_{(0.2 \mu\text{m} - 30 \text{ kDa}) - < 5 \text{ kDa}}$  values ( $-0.33 \pm 0.08\text{‰}$ ) which can be therefore explained by the Fe-OM complexation process.

The lowest  $\delta^{56}\text{Fe}$  was found in the 0.2  $\mu\text{m}$  - 30 kDa fraction. In this fraction, Fe mainly occurred as Fe(III) nano-oxides embedded in humic substances; the dominant process was therefore precipitation as nano-oxides. Our previous results in the OM-free experiment demonstrated that abiotic precipitation did not produce any Fe isotope fractionation. These Fe(III) nano-oxides were formed from the oxidation/hydrolysis of Fe(II)-OM complexes produced during the soil reduction. However, in natural soils, Fe oxidation is mainly catalyzed by heterotrophic or autotrophic Fe(II)-oxidizing bacteria (e.g. *Gallionella*, *Leptothrix*) (e.g. *Wang et al., 2009*). Microbial Fe(II) oxidation is an effective mechanism fractionating Fe isotopes, with the production of isotopically heavy Fe(III) oxyhydroxides relative to the Fe(II) in solution (e.g. *Croal et al., 2004; Balci et al., 2006*).

Mass balance calculation resulted in negative Fe isotopic fractionations  $\Delta^{56}\text{Fe}_{(5 \mu\text{m} - 0.2 \mu\text{m}) - < 5 \text{ kDa}} = -0.24 \pm 0.08\text{‰}$  and  $\Delta^{56}\text{Fe}_{(0.2 \mu\text{m} - 30 \text{ kDa}) - < 5 \text{ kDa}} = -0.33 \pm 0.08\text{‰}$ . In the < 30 and < 5 kDa fractions, Fe occurring as a monomer was complexed by organic molecules which favored the binding of heavy Fe isotopes (Fig. 8). As a consequence, the precipitated colloidal Fe in the 0.2  $\mu\text{m}$  - 30 kDa fraction were enriched in light Fe isotopes with respect to the smaller fractions. The presence of such Fe(III) nanoparticles was also detected in the > 0.2  $\mu\text{m}$  fraction (*Guénet et al., 2017*). Therefore, why did these fractions not exhibit lower  $\delta^{56}\text{Fe}$ ? The  $\delta^{56}\text{Fe}$  value for the 5-0.2  $\mu\text{m}$  fraction was similar to that of the total soil suspension, and was intermediate between those of the > 5  $\mu\text{m}$  and 0.2  $\mu\text{m}$  - 30 kDa fractions. This is explained by its composition, corresponding to the soil which inherited old Fe(III) oxides, Fe(III) nanoparticles, fresh OM and humic substances (*Guénet et al., 2017*).

The combination of (ultra)filtration with spectroscopic characterization of the 0.2  $\mu\text{m}$  - 30 kDa fraction showed the presence of Fe-OM nano-aggregates and clusters. The small organic nano-aggregates (< 5 kDa) promoted the binding of heavy Fe isotopes resulting in enrichment in light Fe isotopes in the 0.2  $\mu\text{m}$  - 30 kDa fraction. However, when ultrafiltration is not performed, this isotope fractionation is hidden by the large Fe phases.

## 5. Conclusion

Although filtration and ultrafiltration are widely used in field studies notably, to fractionate particles, colloids and soluble fractions, just a few studies focused on the impacts of (ultra)filtration on Fe isotopic fractionation. Therefore, in the present work, our purpose was to study the Fe isotopic fractionation ( $\Delta^{56}\text{Fe}$ ) in response to the (ultra)filtration of mixtures of Fe-OM particles, colloids and complexes synthesized from binding and titration methods at various pH levels. The impact of OM deposition on filter membranes was also investigated.

Experiments with or without OM with significant precipitation provided evidence that abiotic precipitation could not be able to fractionate Fe isotopes, since no significant  $\Delta^{56}\text{Fe}$  values were observed. In all of the experiments where the Fe complexation by OM and /or hydroxyl ligands is expected, even in low proportions, a Fe isotope fractionation was observed irrespective of pH. This fractionation may occur through the preferential complexation of heavy Fe isotopes by OM and/or hydroxyl ligands to form stronger chemical bonds (Roe *et al.*, 2003; Dideriksen *et al.*, 2008; Morgan *et al.*, 2010). At low pH, the strong positive fractionation between the  $> 0.2 \mu\text{m}$  and the  $< 0.2 \mu\text{m}$  fractions resulted in a decrease in  $\delta^{56}\text{Fe}$  in the  $< 0.2 \mu\text{m}$  fractions, i.e. a decrease in the amount of heavy Fe isotopes may be in response to the preferential binding of heavy Fe by the OM molecules of the  $> 0.2 \mu\text{m}$  fraction. By contrast, at circum-neutral pH, Fe complexation with small organic matter contained in the  $< 30 \text{ kDa}$  fractions dominated Fe speciation, therefore involving a small increase in  $\delta^{56}\text{Fe}$  potentially in response to the preferential complexation of heavy Fe isotopes by OM.

The OM deposition experiment revealed that regardless of the pH condition, OM deposition indirectly fractionated the Fe isotopes in response to the Fe complexation by OM, which coated the membrane. However, this process is probably very insignificant with regards to the Fe speciation in natural solutions since the complexation occurred before filtration and the Fe speciation is not expected to change during filtration.

These results were used to study and explain the Fe isotope fractionation observed between the various fractions of "natural" Fe-OM associations obtained from the oxidation of a natural reduced soil solution produced by anoxic incubation in a wetland soil. The highest  $\delta^{56}\text{Fe}$  value was obtained in the smallest fraction, i.e. the  $< 5 \text{ kDa}$  fraction, can be due to Fe(III) complexation by small humic OM molecules as monomers or small clusters. The lowest  $\delta^{56}\text{Fe}$  value was determined for the  $0.2 \mu\text{m} - 30 \text{ kDa}$  fraction, where Fe mainly occurred

as Fe(III) nano-particles embedded within the humic organic matrix. Regarding the results stemming from this study, this low  $\delta^{56}\text{Fe}$  value can result from the strong complexes formed by heavy Fe and organic molecules in the smallest fractions.

This observation of such Fe isotopic fractionation notably, for “natural” Fe-OM associations, was only possible through the use of the fractionation method, which allowed the discrimination of the prevailing chemical processes. Therefore, this method should be extensively used in the study of Fe fractionation since, neither filtration, nor ultrafiltration fractionated Fe isotopes. It appears that filtration and ultrafiltration are essential for further experimental and field studies, in order to assess Fe and OM speciation in the different fractions and therefore help to understand the potential control of the Fe isotopic fractionation.

### Acknowledgements

We thank Patrice Petitjean and Alexis Duprunelle for performing the DOC and the iron isotope analyses (using MC-ICPMS at IFREMER in Brest), respectively. Dr. S. Mullin is acknowledged for post-editing the English style (<https://www.proz.com/profile/677614>). This work was supported by a CNRS-EC2CO grant, named ISO-TRANS-FER. The authors would also like to thank all 3 anonymous reviewers for their help and advice.

### REFERENCES

- Abadie C., Lacan F., Radic A., Pradoux C. and Poitrasson F. (2017) Iron isotopes reveal distinct dissolved iron sources and pathways in the intermediate versus deep Southern Ocean. *Proc. Natl. Acad. Sci.* **114**, 858–863.
- Allard T., Menguy N., Salomon J., Calligaro T., Weber T., Calas G. and Benedetti M. F. (2004) Revealing forms of iron in river-borne material from major tropical rivers of the Amazon Basin (Brazil). *Geochim. Cosmochim. Acta* **68**, 3079–3094.
- Balci N., Bullen T. D., Witte-Lien K., Shanks W. C., Motelica M. and Mandernack K. W. (2006) Iron isotope fractionation during microbially stimulated Fe(II) oxidation and Fe(III) precipitation. *Geochim. Cosmochim. Acta* **70**, 622–639.
- Bullen T. D., White A. F., Childs C. W., Vivit D. V. and Schulz M. S. (2001) Demonstration of significant abiotic iron isotope fractionation in nature. *Geology* **29**, 699–702.
- Catrouillet C., Davranche M., Dia A., Bouhnik-Le Coz M., Marsac R., Pourret O. and Gruau G. (2014) Geochemical modeling of Fe(II) binding to humic and fulvic acids. *Chem. Geol.* **372**, 109–118.

- Chen J.-B., Busigny V., Gaillardet J., Louvat P. and Wang Y.-N. (2014) Iron isotopes in the Seine River (France): Natural versus anthropogenic sources. *Geochim. Cosmochim. Acta* **128**, 128–143.
- Conway T. M. and John S. G. (2014) Quantification of dissolved iron sources to the North Atlantic Ocean. *Nature* **511**, 212.
- Croal L. R., Johnson C. M., Beard B. L. and Newman D. K. (2004) Iron isotope fractionation by Fe(II)-oxidizing photoautotrophic bacteria. *Geochim. Cosmochim. Acta* **68**, 1227–1242.
- Crosby H. A., Roden E. E., Johnson C. M. and Beard B. L. (2007) The mechanisms of iron isotope fractionation produced during dissimilatory Fe(III) reduction by *Shewanella putrefaciens* and *Geobacter sulfurreducens*. *Geobiology* **5**, 169–189.
- Dauphas N., John S. G. and Rouxel O. (2017) Iron Isotope Systematics. *Rev. Mineral. Geochem.* **82**, 415–510.
- Davranche M., Dia A., Fakhri M., Nowack B., Gruau G., Ona-anguema G., Petitjean P., Martin S. and Hochreutener R. (2013) Organic matter control on the reactivity of Fe(III)-oxyhydroxides and associated As in wetland soils: A kinetic modeling study. *Chem. Geol.* **335**, 24–35.
- Dideriksen K., Baker J. A. and Stipp S. L. S. (2008) Equilibrium Fe isotope fractionation between inorganic aqueous Fe(III) and the siderophore complex, Fe(III)-desferrioxamine B. *Earth Planet. Sci. Lett.* **269**, 280–290.
- Escoube R., Rouxel O. J., Pokrovsky O. S., Schroth A., Max Holmes R. and Donard O. F. X. (2015) Iron isotope systematics in Arctic rivers. *Comptes Rendus Geosci.* **347**, 377–385.
- Escoube R., Rouxel O. J., Sholkovitz E. and Donard O. F. X. (2009) Iron isotope systematics in estuaries: The case of North River, Massachusetts (USA). *Geochim. Cosmochim. Acta* **73**, 4045–4059.
- Fitzsimmons J. N., Carrasco G. G., Wu J., Roshan S., Hatta M., Measures C. I., Conway T. M., John S. G. and Boyle E. A. (2015) Partitioning of dissolved iron and iron isotopes into soluble and colloidal phases along the GA03 GEOTRACES North Atlantic Transect. *Deep Sea Res. Part II Top. Stud. Oceanogr.* **116**, 130–151.
- Fitzsimmons J. N., Conway T. M., Lee J.-M., Kayser R., Thyng K. M., John S. G. and Boyle E. A. (2016) Dissolved iron and iron isotopes in the southeastern Pacific Ocean. *Glob. Biogeochem. Cycles* **30**, 1372–1395.
- Friedrich A. J., Beard B. L., Reddy T. R., Scherer M. M. and Johnson C. M. (2014) Iron isotope fractionation between aqueous Fe(II) and goethite revisited: New insights based on a multi-direction approach to equilibrium and isotopic exchange rate modification. *Geochim. Cosmochim. Acta* **139**, 383–398.

- Grybos M., Davranche M., Gruau G. and Petitjean P. (2007) Is trace metal release in wetland soils controlled by organic matter mobility or Fe-oxyhydroxides reduction? *J. Colloid Interface Sci.* **314**, 490–501.
- Guénet H., Davranche M., Vantelon D., Bouhnik-Le Coz M., Jardé E., Pierson-Wickmann A. C., Dorcet V., Demangeat E. and Jestin J. (2017) Highlighting the wide variability in arsenic speciation in wetlands: A new insight into the control of the behavior of arsenic. *Geochim. Cosmochim. Acta* **203**, 284–302.
- Guénet H., Davranche M., Vantelon D., Pédrot M., Al-Sid-Cheikh M., Dia A. and Jestin J. (2016) Evidence of organic matter control on As oxidation by iron oxides in riparian wetlands. *Chem. Geol.* **439**, 161–172.
- Hirst C., Andersson P. S., Shaw S., Burke I. T., Kutscher L., Murphy M. J., Maximov T., Pokrovsky O. S., Mörtz C.-M. and Porcelli D. (2017) Characterisation of Fe-bearing particles and colloids in the Lena River basin, NE Russia. *Geochim. Cosmochim. Acta* **213**, 553–573.
- Icopini G. A., Anbar A. D., Ruebush S. S., Tien M. and Brantley S. L. (2004) Iron isotope fractionation during microbial reduction of iron: The importance of adsorption. *Geology* **32**, 205–208.
- Ilna S. M., Poitrasson F., Lapitskiy S. A., Alekhin Y. V., Viers J. and Pokrovsky O. S. (2013) Extreme iron isotope fractionation between colloids and particles of boreal and temperate organic-rich waters. *Geochim. Cosmochim. Acta* **101**, 96–111.
- Jeitner T. M. (2014) Optimized ferrozine-based assay for dissolved iron. *Anal. Biochem.* **454**, 36–37.
- Johnson C. M., Beard B. L. and Roden E. E. (2008) The Iron Isotope Fingerprints of Redox and Biogeochemical Cycling in Modern and Ancient Earth. *Annu. Rev. Earth Planet. Sci.* **36**, 457–493.
- Johnson C. M., Skulan J. L., Beard B. L., Sun H., Nealson K. H. and Braterman P. S. (2002) Isotopic fractionation between Fe (III) and Fe (II) in aqueous solutions. *Earth Planet. Sci. Lett.* **195**, 141–153.
- Lambert T., Pierson-Wickmann A.-C., Gruau G., Jaffrezic A., Petitjean P., Thibault J. N. and Jeanneau L. (2014) DOC sources and DOC transport pathways in a small headwater catchment as revealed by carbon isotope fluctuation during storm events. *Biogeosciences* **11**, 3043–3056.
- Liang L., Moline G. R., Kamolpornwijit W. and West O. R. (2005) Influence of hydrogeochemical processes on zero-valent iron reactive barrier performance: A field investigation. *J. Contam. Hydrol.* **80**, 71–91.
- Manasyrov R. M., Vorobyev S. N., Loiko S. V., Kritzkov I. V., Shirokova L. S., Shevchenko V. P., Kirpotin S. N., Kulizhsky S. P., Kolesnichenko L. G., Zemtsov V. A., Sinkin V. V. and Pokrovsky O. S. (2015) Seasonal dynamics of organic carbon and metals in

- thermokarst lakes from the discontinuous permafrost zone of western Siberia. *Biogeosciences* **12**, 3009–3028.
- Marsac R., Davranche M., Gruau G., Bouhnik-Le Coz M. and Dia A. (2011) An improved description of the interactions between rare earth elements and humic acids by modeling: PHREEQC-Model VI coupling. *Geochim. Cosmochim. Acta* **75**, 5625–5637.
- Marsac R., Davranche M., Gruau G., Dia A., Pédrot M., Le Coz-Bouhnik M. and Briant N. (2013) Effects of Fe competition on REE binding to humic acid: Origin of REE pattern variability in organic waters. *Chem. Geol.* **342**, 119–127.
- Morgan J. L. L., Wasylenki L. E., Nuester J. and Anbar A. D. (2010) Fe isotope fractionation during equilibration of Fe-organic complexes. *Environ. Sci. Technol.* **44**, 6095–6101.
- Neubauer E., von der Kammer F., Knorr K.-H., Peiffer S., Reichert M. and Hofmann T. (2013) Colloid-associated export of arsenic in stream water during stormflow events. *Chem. Geol.* **352**, 81–91.
- Pédrot M., Dia A., Davranche M., Bouhnik-Le Coz M., Henin O. and Gruau G. (2008) Insights into colloid-mediated trace element release at the soil/water interface. *J. Colloid Interface Sci.* **325**, 187–197.
- Pokrovsky O. S., Dupré B. and Schott J. (2005) Fe–Al–organic Colloids Control of Trace Elements in Peat Soil Solutions: Results of Ultrafiltration and Dialysis. *Aquat. Geochem.* **11**, 241–278.
- Pokrovsky O. S. and Schott J. (2002) Iron colloids/organic matter associated transport of major and trace elements in small boreal rivers and their estuaries (NW Russia). *Chem. Geol.* **190**, 141–179.
- Roe J. E., Anbar A. D. and Barling J. (2003) Nonbiological fractionation of Fe isotopes: Evidence of an equilibrium isotope effect. *Chem. Geol.* **195**, 69–85.
- Rouxel O. J. and Auro M. (2010) Iron Isotope Variations in Coastal Seawater Determined by Multicollector ICP-MS. *Geostand. Geoanalytical Res.* **34**, 135–144.
- Rouxel O., Sholkovitz E., Charette M. and Edwards K. J. (2008) Iron isotope fractionation in subterranean estuaries. *Geochim. Cosmochim. Acta* **72**, 3413–3430.
- Rouxel O., Toner B. M., Manganini S. J. and German C. R. (2016) Geochemistry and iron isotope systematics of hydrothermal plume fall-out at East Pacific Rise 9°50'N. *Chem. Geol.* **441**, 212–234.
- dos Santos Pinheiro G. M., Poitrasson F., Sondag F., Cochonneau G. and Vieira L. C. (2014) Contrasting iron isotopic compositions in river suspended particulate matter: the Negro and the Amazon annual river cycles. *Earth Planet. Sci. Lett.* **394**, 168–178.
- Schroth A. W., Crusius J., Chever F., Bostick B. C. and Rouxel O. J. (2011) Glacial influence on the geochemistry of riverine iron fluxes to the Gulf of Alaska and effects of

deglaciation. *Geophysicl. Res. Lett.* **38**. Available at: <https://doi.org/10.1029/2011GL048367> [Accessed November 23, 2018].

- Shirokova L. S., Pokrovsky O. S., Kirpotin S. N., Desmukh C., Pokrovsky B. G., Audry S. and Viers J. (2013) Biogeochemistry of organic carbon, CO<sub>2</sub>, CH<sub>4</sub>, and trace elements in thermokarst water bodies in discontinuous permafrost zones of Western Siberia. *Biogeochemistry* **113**, 573–593.
- Sholkovitz E. R. (1976) Flocculation of dissolved organic and inorganic matter during the mixing of river water and seawater. *Geochim. Cosmochim. Acta* **40**, 831–845.
- Sigg L., Behra P., Stumm W., Sigg L. M., Chemist S. and Chemist F. (2014) *Chimie des milieux aquatiques.*,
- Skulan J., Beard B. and Johnson C. (2002) Kinetic and equilibrium Fe isotope fractionation between aqueous Fe (III) and hematite. *Geochim. Cosmochim. Acta* **66**, 2995–3015.
- Stookey L. L. (1970) Ferrozine-a new spectrophotometric reagent for iron. *Analytical Chemistry* **42**, 779-781.
- Teutsch N., von Gunten U., Porcelli D., Cirpka O. A. and Halliday A. N. (2005) Adsorption as a cause for iron isotope fractionation in reduced groundwater. *Geochim. Cosmochim. Acta* **69**, 4175–4185.
- Wang J., Muyzer G., Bodelier P. L. E. and Laanbroek H. J. (2009) Diversity of iron oxidizers in wetland soils revealed by novel 16S rRNA primers targeting Gallionella-related bacteria. *ISME J.* **3**, 715–725.
- Weber T., Allard T., Tipping E. and Benedetti M. F. (2006) Modeling Iron Binding to Organic Matter. *Environ. Sci. Technol.* **40**, 7488–7493.
- Welch S. A., Beard B. L., Johnson C. M. and Braterman P. S. (2003) Kinetic and equilibrium Fe isotope fractionation between aqueous Fe(II) and Fe(III). *Geochim. Cosmochim. Acta* **67**, 4231–4250.
- Wiederhold J. G., Teutsch N., Kraemer S. M., Halliday A. N. and Kretzschmar R. (2007) Iron isotope fractionation in oxic soils by mineral weathering and podzolization. *Geochim. Cosmochim. Acta* **71**, 5821–5833.
- Wu L., Percak-Dennett E. M., Beard B. L., Roden E. E. and Johnson C. M. (2012) Stable iron isotope fractionation between aqueous Fe(II) and model Archean ocean Fe–Si coprecipitates and implications for iron isotope variations in the ancient rock record. *Geochim. Cosmochim. Acta* **84**, 14–28.

**Figure Captions:**

Fig. 1. The Fe percentage (a) and the  $\delta^{56}\text{Fe}$  (b) relative to the size fractions (total,  $< 0.2 \mu\text{m}$ ,  $< 30 \text{kDa}$  and  $< 5 \text{kDa}$ ) in the OM-free experiments at pH 1, 2 and 6.5.

Fig. 2. The DOC relative to the size fractions (total,  $< 0.2 \mu\text{m}$ ,  $< 30 \text{kDa}$  and  $< 5 \text{kDa}$ ) in the Fe-free experiments at pH 2 and 6.5.

Fig. 3. The Fe percentage (a), DOC (b) and the  $\delta^{56}\text{Fe}$  (c) relative to the size fractions (total,  $< 0.2 \mu\text{m}$ ,  $< 30 \text{kDa}$  and  $< 5 \text{kDa}$ ) in the Fe-OM binding experiment at pH 1, 2 and 6.5.

Fig. 4. The Fe percentage (a), DOC (b) and the  $\delta^{56}\text{Fe}$  (c) relative to the size fractions (total,  $< 0.2 \mu\text{m}$ ,  $< 30 \text{kDa}$  and  $< 5 \text{kDa}$ ) in the OM titration by Fe at pH 2 and 6.5.

Fig. 5. The Fe percentage (a), DOC (b) and the  $\delta^{56}\text{Fe}$  (c) relative to the size fractions (total,  $< 0.2 \mu\text{m}$ ,  $< 30 \text{kDa}$  and  $< 5 \text{kDa}$ ) in the OM deposition experiment at pH 2 and 6.5.

Fig. 6. The Fe percentage (a), DOC (b) and the  $\delta^{56}\text{Fe}$  (c) relative to the size fractions (total,  $> 5 \mu\text{m}$ ,  $5 \mu\text{m} - 0.2 \mu\text{m}$ ,  $0.2 \mu\text{m} - 30 \text{kDa}$ ,  $< 30 \text{kDa}$  and  $< 5 \text{kDa}$ ) in natural Fe-OM associations.

Fig. 7. The  $\delta^{56}\text{Fe}$  of the total (square),  $< 0.2 \mu\text{m}$  (triangle) and  $< 30 \text{kDa}$  (circle) fractions for the Fe-OM experiments relative to the Fe concentration ( $\mu\text{mol L}^{-1}$ ) at pH 6.5. The gray zone illustrates from the minimum ( $48 \pm 0.03\text{‰}$ ) to the maximum ( $0.61 \pm 0.05\text{‰}$ ) of  $\delta^{56}\text{Fe}$  values in the total fractions.

Fig. 8. Transmission electron microscopy micrographs of the fractions. a) Large view of the  $> 0.2 \mu\text{m}$  fraction. b) Close-up on a Fe aggregate corresponding to the red square from micrograph a. c) micrograph of the  $0.2 \mu\text{m} - 30 \text{kDa}$  fraction.

Fig. 9. The  $\delta^{56}\text{Fe}$  of the natural Fe-OM associations relative to Fe percentage.

**Table 1** - Chemical and isotopic compositions of filtrates and ultrafiltrates for the OM-free experiment.

OM-free pH 1						
Size fraction	[Fe] $\mu\text{mol L}^{-1}$	[Fe] (%)	$\delta^{56}\text{Fe}$ (‰)	2 $\sigma$ (%)	$\delta^{56}\text{Fe}'$ (‰)	2 $\sigma'$ (‰)
Total	97 $\pm$ 2		0.57	0.05		
> 0.2 $\mu\text{m}^*$	4.8 $\pm$ 2.8	4.9 $\pm$ 2.9	nd.	nd.	nd.	nd.
< 0.2 $\mu\text{m}$	92 $\pm$ 2	95 $\pm$ 3	0.55	0.05	-0.01	0.08
> 30 kDa*	6.5 $\pm$ 2.8	6.7 $\pm$ 2.9	nd.	nd.	nd.	nd.
< 30 kDa	90 $\pm$ 2	93 $\pm$ 3	0.50	0.05	-0.06	0.08
> 5 kDa*	7.7 $\pm$ 2.8	8.0 $\pm$ 2.9	nd.	nd.	nd.	nd.
< 5 kDa	89 $\pm$ 2	92 $\pm$ 3	0.54	0.05	-0.02	0.08
0.2 $\mu\text{m}$ - 30 kDa*	1.7 $\pm$ 2.7	1.8 $\pm$ 2.8	nd.	nd.	nd.	nd.
30 -5 kDa*	1.2 $\pm$ 2.7	1.3 $\pm$ 2.8	nd.	nd.	nd.	nd.
OM- free pH 2						
Size fraction	[Fe] $\mu\text{mol L}^{-1}$	[Fe] (%)	$\delta^{56}\text{Fe}$ (‰)	2 $\sigma$ (%)	$\delta^{56}\text{Fe}'$ (‰)	2 $\sigma'$ (‰)
Total	91 $\pm$ 2		0.61	0.03		
> 0.2 $\mu\text{m}^*$	7.2 $\pm$ 2.6	7.9 $\pm$ 2.9	-0.33	0.66	-0.94	0.66
< 0.2 $\mu\text{m}$	83 $\pm$ 2	92 $\pm$ 3	0.68	0.03	0.08	0.04
> 30 kDa*	14 $\pm$ 2	16 $\pm$ 3	nd.	nd.	nd.	nd.
< 30 kDa	76 $\pm$ 2	84 $\pm$ 2	0.75	0.03	0.14	0.04
> 5 kDa*	17 $\pm$ 2	19 $\pm$ 3	nd.	nd.	nd.	nd.
< 5 kDa	73 $\pm$ 4	80 $\pm$ 2	0.83	0.03	0.22	0.04
0.2 $\mu\text{m}$ - 30 kDa*	7.5 $\pm$ 2.4	8.3 $\pm$ 2.6	nd.	nd.	nd.	nd.
30 -5 kDa*	2.6 $\pm$ 2.2	2.9 $\pm$ 2.5	nd.	nd.	nd.	nd.
OM-free pH 6.5						
Size fraction	[Fe] $\mu\text{mol L}^{-1}$	[Fe] (%)	$\delta^{56}\text{Fe}$ (‰)	2 $\sigma$ (%)	$\delta^{56}\text{Fe}'$ (‰)	2 $\sigma'$ (‰)
Total	40 $\pm$ 1		0.61	0.05		
> 0.2 $\mu\text{m}^*$	26 $\pm$ 1	65 $\pm$ 3	0.64	0.08	0.03	0.10
< 0.2 $\mu\text{m}$	14 $\pm$ 0.3	35 $\pm$ 1	0.55	0.05	-0.06	0.08
< 30 kDa	<LOD	nd.	<LOD	nd.	nd.	nd.
< 5 kDa	<LOD	nd.	<LOD	nd.	nd.	nd.

DOC: dissolved organic carbon. \*: Calculated fraction. <LOD: below limit of detection. nd.: not determined.

**Table 2** - Percentage of Fe-OM binding (**Fe-OM %**), precipitated Fe as ferrihydrite (**Ferrihydrite %**),  $\text{Fe}^{3+}$  and Fe complexed by  $\text{OH}^-$  ( $\text{Fe}(\text{OH})_n^{3-n}$  %) without and with OM, calculated using PHREEQC-Model VI.

OM-free					
pH	DOC mmol L <sup>-1</sup>	Fe-OM %	Ferrihydrite %	Fe <sup>3+</sup> %	[Fe(OH) <sub>n</sub> ] <sup>3-n</sup> %
1	0.0	0.0	0.0	99.9	0.1
2	0.0	0.0	0.0	93.4	6.6
6.5	0.0	0.0	99.9	0.0	0.1
Fe(III)-OM binding					
pH	DOC mmol L <sup>-1</sup>	Fe-OM %	Ferrihydrite %	Fe <sup>3+</sup> %	[Fe(OH) <sub>n</sub> ] <sup>3-n</sup> %
1	4.17	8.7	0.0	91.2	0.1
2	4.17	31.1	0.0	64.2	4.6
6.5	4.17	5.7	94.3	0.0	0.0

**Table 3** - Iron isotopic fractionation between size for the OM-free, Fe-OM binding, titration OM deposition experiments and Fe-OM natural association.

OM-free							
$\Delta^{56}\text{Fe}_{A-B}$	B→	< 0.2 $\mu\text{m}$	0.2 $\mu\text{m}$ -30 kDa	< 30 kDa	30 -5kDa	< 5 kDa	pH
A↓ > 0.2 $\mu\text{m}$		ns.	ns.	ns.	ns.	ns.	1
		-1.01 ± 0.66	ns.	-1.08 ± 0.66	ns.	-1.16 ± 0.66	2
		ns.	nd.	nd.	nd.	nd.	6.5
0.2 $\mu\text{m}$ -30 kDa		--	--	ns.	ns.	--	1
		--	--	-0.72 ± 0.50	ns.	-0.80 ± 0.50	2
		--	--	nd.	nd.	nd.	6.5
30 -5kDa		--	ns.	--	--	ns.	1
		--	ns.	--	--	ns.	2
		--	nd.	--	--	nd.	6.5
Binding							
$\Delta^{56}\text{Fe}_{A-B}$		< 0.2 $\mu\text{m}$	0.2 $\mu\text{m}$ -30 kDa	< 30 kDa	30 -5kDa	< 5 kDa	pH
> 0.2 $\mu\text{m}$		ns.	ns.	ns.	ns.	ns.	1
		0.97 ± 0.11	ns.	0.94 ± 0.11	1.02 ± 0.64	0.94 ± 0.11	2
		-0.12 ± 0.08	-0.11 ± 0.08	-0.40 ± 0.08	nd.	nd.	6.5
0.2 $\mu\text{m}$ -30 kDa		--	--	ns.	ns.	ns.	1
		--	--	ns.	ns.	ns.	2
		--	--	-0.29 ± 0.05	nd.	nd.	6.5
30 -5kDa		--	ns.	--	--	ns.	1
		--	ns.	--	--	ns.	2
		--	nd.	--	--	nd.	6.5
Titration							
$\Delta^{56}\text{Fe}_{A-B}$		< 0.2 $\mu\text{m}$	0.2 $\mu\text{m}$ -30 kDa	< 30 kDa	30 -5kDa	< 5 kDa	pH
> 0.2 $\mu\text{m}$		3.04 ± 0.62	2.78 ± 0.91	3.02 ± 0.62	ns.	3.02 ± 0.62	2
		ns.	ns.	-0.32 ± 0.11	nd.	nd.	6.5
0.2 $\mu\text{m}$ -30 kDa		--	--	ns.	ns.	ns.	2
		--	--	-0.23 ± 0.05	nd.	nd.	6.5
30 -5kDa		--	ns.	--	--	ns.	2
		--	nd.	--	--	nd.	6.5
OM deposition							
$\Delta^{56}\text{Fe}_{A-B}$		< 0.2 $\mu\text{m}$	0.2 $\mu\text{m}$ -30 kDa	< 30 kDa	30 -5kDa	< 5 kDa	pH
> 0.2 $\mu\text{m}$		ns.	ns.	ns.	-3.12 ± 1.34	0.21 ± 0.09	2
		0.39 ± 0.06	nd.	nd.	nd.	nd.	6.5
0.2 $\mu\text{m}$ -30 kDa		--	--	ns.	-3.09 ± 1.34	0.24 ± 0.07	2
		--	--	nd.	nd.	nd.	6.5
30 -5kDa		--	3.09 ± 1.34	--	--	3.33 ± 1.34	2
		--	nd.	--	--	nd.	6.5

Fe -OM natural association				
$\Delta^{56}\text{Fe}_{\text{A-B}}$	5-0.2 $\mu\text{m}$	0.2 $\mu\text{m}$ -30 kDa	30 - 5 kDa	< 5 kDa
> 5 $\mu\text{m}$	0.16 $\pm$ 0.05	0.26 $\pm$ 0.04	0.21 $\pm$ 0.09	ns.
5-0.2 $\mu\text{m}$	---	0.10 $\pm$ 0.04	-0.18 $\pm$ 0.04	-0.24 $\pm$ 0.08
0.2 $\mu\text{m}$ -30 kDa	-0.10 $\pm$ 0.04	---	-0.28 $\pm$ 0.04	-0.33 $\pm$ 0.08
30 - 5 kDa	0.18 $\pm$ 0.04	0.28 $\pm$ 0.04	---	ns.

---: Not defined isotopic fractionation. ns. : No significant error propagation. nd. : not determined.

**Table 4** - Chemical and isotopic compositions of filtrates and ultrafiltrates for the Fe-free experiment.

Fe-free pH 2					
Size fraction	[Fe] $\mu\text{mol L}^{-1}$	DOC $\text{mmol L}^{-1}$	DOC (%)	$\delta^{56}\text{Fe}$ (‰)	$2\sigma$ (‰)
Total	9.6 $\pm$ 0.2	3.6 $\pm$ 0.1		0.11	0.04
> 0.2 $\mu\text{m}^*$	nd.	2.0 $\pm$ 1	56 $\pm$ 4	nd.	nd.
< 0.2 $\mu\text{m}$	<LOD	1.6 $\pm$ 0.1	43 $\pm$ 2	nd.	nd.
> 30 kDa*	nd.	2.5 $\pm$ 0.1	68 $\pm$ 4	nd.	nd.
< 30 kDa	<LOD	1.15 $\pm$ 0.04	32 $\pm$ 2	nd.	nd.
> 5 kDa*	nd.	2.6 $\pm$ 0.1	72 $\pm$ 4	nd.	nd.
< 5 kDa	<LOD	1.02 $\pm$ 0.04	28 $\pm$ 1	nd.	nd.
0.2 $\mu\text{m}$ - 30 kDa*	nd.	0.43 $\pm$ 0.07	12 $\pm$ 2	nd.	nd.
30 -5 kDa*	nd.	0.13 $\pm$ 0.05	3.5 $\pm$ 1.5	nd.	nd.
Fe-free pH 6.5					
Size fraction	[Fe] $\mu\text{mol L}^{-1}$	DOC $\text{mmol L}^{-1}$	DOC (%)	$\delta^{56}\text{Fe}$ (‰)	$2\sigma$ (‰)
Total	7.3 $\pm$ 0.1	3.9 $\pm$ 0.1		0.07	0.04
> 0.2 $\mu\text{m}^*$	nd.	0.8 $\pm$ 0.2	20 $\pm$ 5	nd.	nd.
< 0.2 $\mu\text{m}$	<LOD	3 $\pm$ 0.1	80 $\pm$ 4	nd.	nd.
> 30 kDa*	nd.	2.3 $\pm$ 0.2	58 $\pm$ 4	nd.	nd.
< 30 kDa	<LOD	1.6 $\pm$ 0.1	42 $\pm$ 2	nd.	nd.
> 5 kDa*	nd.	3.3 $\pm$ 0.1	85 $\pm$ 5	nd.	nd.
< 5 kDa	<LOD	0.58 $\pm$ 0.02	15 $\pm$ 1	nd.	nd.
0.2 $\mu\text{m}$ - 30 kDa*	nd.	3.1 $\pm$ 0.1	80 $\pm$ 4	nd.	nd.
30 -5 kDa*	nd.	1.1 $\pm$ 0.1	27 $\pm$ 2	nd.	nd.

DOC: dissolved organic carbon. \*: Calculated fraction. <LOD: below limit of detection. nd.: not determined.

**Table 5** - Chemical and isotopic compositions of filtrates and ultrafiltrates for the Fe-OM binding experiment.

Binding pH 1								
Size fraction	[Fe] $\mu\text{mol L}^{-1}$	[Fe] (%)	DOC $\text{mmol L}^{-1}$	DOC (%)	$\delta^{56}\text{Fe}$ (‰)	2 $\sigma$ (‰)	$\delta^{56}\text{Fe}'$ (‰)	2 $\sigma'$ (‰)
Total	86 $\pm$ 2		3.7 $\pm$ 0.1		0.54	0.04		
> 0.2 $\mu\text{m}^*$	2.3 $\pm$ 2	2.6 $\pm$ 3.0	2.8 $\pm$ 0.1	76 $\pm$ 4	nd.	nd.	nd.	nd.
< 0.2 $\mu\text{m}$	83 $\pm$ 2	97 $\pm$ 3	0.88 $\pm$ 0.03	24 $\pm$ 1	0.54	0.04	-0.01	0.06
> 30 kDa*	7.2 $\pm$ 2.5	8.4 $\pm$ 2.9	2.8 $\pm$ 0.1	76 $\pm$ 4	nd.	nd.	nd.	nd.
< 30 kDa	78 $\pm$ 2	92 $\pm$ 3	0.88 $\pm$ 0.08	24 $\pm$ 1	0.44	0.05	-0.11	0.07
> 5 kDa*	8.2 $\pm$ 2.4	9.6 $\pm$ 2.9	2.8 $\pm$ 0.1	77 $\pm$ 4	nd.	nd.	nd.	nd.
< 5 kDa	77 $\pm$ 2	90 $\pm$ 2.7	0.82 $\pm$ 0.03	22 $\pm$ 1	0.45	0.05	-0.10	0.07
0.2 $\mu\text{m}$ - 30 kDa*	4.9 $\pm$ 2.4	5.8 $\pm$ 2.8	0.01 $\pm$ 0.04	0.2 $\pm$ 1.2	nd.	nd.	nd.	nd.
30 -5 kDa*	1.0 $\pm$ 2.3	1.2 $\pm$ 2.7	0.05 $\pm$ 0.04	1.5 $\pm$ 1.2	nd.	nd.	nd.	nd.
Binding pH 2								
Size fraction	[Fe] $\mu\text{mol L}^{-1}$	[Fe] (%)	DOC $\text{mmol L}^{-1}$	DOC (%)	$\delta^{56}\text{Fe}$ (‰)	2 $\sigma$ (‰)	$\delta^{56}\text{Fe}'$ (‰)	2 $\sigma'$ (‰)
Total	109 $\pm$ 2		3.4 $\pm$ 0.1		0.53	0.05		
> 0.2 $\mu\text{m}^*$	53 $\pm$ 3	49 $\pm$ 3	3.1 $\pm$ 0.1	90 $\pm$ 5	1.02	0.10	0.49	0.11
< 0.2 $\mu\text{m}$	55 $\pm$ 1	51 $\pm$ 1	0.34 $\pm$ 0.01	9.9 $\pm$ 0.5	0.05	0.05	-0.48	0.06
> 30 kDa*	56 $\pm$ 3	52 $\pm$ 3	3.1 $\pm$ 0.1	91 $\pm$ 5	0.94	0.09	0.41	0.10
< 30 kDa	52 $\pm$ 1	48 $\pm$ 1	0.29 $\pm$ 0.01	8.6 $\pm$ 0.4	0.08	0.05	-0.45	0.06
> 5 kDa*	61 $\pm$ 2	57 $\pm$ 3	3.1 $\pm$ 0.1	92 $\pm$ 5	0.86	0.09	0.33	0.10
< 5 kDa	47 $\pm$ 1	43 $\pm$ 1	0.28 $\pm$ 0.01	8.3 $\pm$ 0.4	0.08	0.05	-0.44	0.06
0.2 $\mu\text{m}$ - 30 kDa*	2.9 $\pm$ 1.6	2.6 $\pm$ 1.5	0.04 $\pm$ 0.02	1.3 $\pm$ 0.5	nd.	nd.	nd.	nd.
30 -5 kDa*	5.3 $\pm$ 1.5	4.8 $\pm$ 1.4	0.01 $\pm$ 0.01	0.3 $\pm$ 0.4	nd.	nd.	nd.	nd.
Binding pH 6.5								
Size fraction	[Fe] $\mu\text{mol L}^{-1}$	[Fe] (%)	DOC $\text{mmol L}^{-1}$	DOC (%)	$\delta^{56}\text{Fe}$ (‰)	2 $\sigma$ (‰)	$\delta^{56}\text{Fe}'$ (‰)	2 $\sigma'$ (‰)
Total	69 $\pm$ 1		4.3 $\pm$ 0.1		0.48	0.03		
>0.2 $\mu\text{m}^*$	40 $\pm$ 2	57 $\pm$ 3	1.8 $\pm$ 0.2	42 $\pm$ 4	0.43	0.07	-0.05	0.08
< 0.2 $\mu\text{m}$	30 $\pm$ 1	43 $\pm$ 1	2.5 $\pm$ 0.01	57 $\pm$ 3	0.55	0.04	0.07	0.05
> 30 kDa*	nd.	nd.	3.5 $\pm$ 0.2	80 $\pm$ 5	0.48	0.03	0.00	0.05
< 30 kDa	0.58 $\pm$ 0.02	0.84 $\pm$ 0.03	0.86 $\pm$ 0.03	20 $\pm$ 1	0.83	0.03	0.35	0.05
> 5 kDa*	nd.	nd.	3.9 $\pm$ 0.1	89 $\pm$ 5	nd.	nd.	nd.	nd.
< 5 kDa	<LOD	nd.	0.46 $\pm$ 0.02	10.6 $\pm$ 0.5	nd.	nd.	nd.	nd.
0.2 $\mu\text{m}$ - 30 kDa*	29 $\pm$ 1	42 $\pm$ 1	1.6 $\pm$ 0.1	38 $\pm$ 2	0.54	0.04	0.06	0.05
30 -5 kDa*	nd.	nd.	0.39 $\pm$ 0.03	9.1 $\pm$ 0.9	nd.	nd.	nd.	nd.

DOC: dissolved organic carbon. \*: Calculated fraction. <LOD: below limit of detection. nd.: not determined.

**Table 6** - Chemical and isotopic compositions of filtrates and ultrafiltrates for the Fe-OM titration experiment.

Titration pH 2								
Size fraction	[Fe] $\mu\text{mol L}^{-1}$	[Fe] (%)	DOC $\text{mmol L}^{-1}$	DOC (%)	$\delta^{56}\text{Fe}$ (‰)	2 $\sigma$ (‰)	$\delta^{56}\text{Fe}'$ (‰)	2 $\sigma'$ (‰)
Total	81 $\pm$ 2		4.3 $\pm$ 0.1		0.55	0.03		
> 0.2 $\mu\text{m}^*$	13 $\pm$ 2	16 $\pm$ 3	3.4 $\pm$ 0.1	80 $\pm$ 3	3.10	0.62	2.55	0.62
< 0.2 $\mu\text{m}$	68 $\pm$ 1	84 $\pm$ 2	0.86 $\pm$ 0.03	20.2 $\pm$ 0.9	0.06	0.04	-0.49	0.06
> 30 kDa*	19 $\pm$ 2	24 $\pm$ 3	3.5 $\pm$ 0.1	81 $\pm$ 3	2.12	0.32	1.57	0.32
< 30 kDa	62 $\pm$ 1	76 $\pm$ 2	0.80 $\pm$ 0.03	18.9 $\pm$ 0.8	0.08	0.04	-0.48	0.06
> 5 kDa*	19 $\pm$ 2	24 $\pm$ 3	3.5 $\pm$ 0.1	81 $\pm$ 3	2.08	0.30	1.53	0.30
< 5 kDa	62 $\pm$ 1	76 $\pm$ 2	0.79 $\pm$ 0.03	18.6 $\pm$ 0.8	0.08	0.04	-0.48	0.06
0.2 $\mu\text{m}$ - 30 kDa*	6.7 $\pm$ 2.0	8.3 $\pm$ 2.4	0.06 $\pm$ 0.04	1 $\pm$ 1	nd.	nd.	nd.	nd.
30 -5 kDa*	0 $\pm$ 2	nd.	0.01 $\pm$ 0.04	0.3 $\pm$ 0.9	nd.	nd.	nd.	nd.
Titration pH 6.5								
Size fraction	[Fe] $\mu\text{mol L}^{-1}$	[Fe] (%)	DOC $\text{mmol L}^{-1}$	DOC (%)	$\delta^{56}\text{Fe}$ (‰)	2 $\sigma$ (‰)	$\delta^{56}\text{Fe}'$ (‰)	2 $\sigma'$ (‰)
Total	57 $\pm$ 1		4.4 $\pm$ 0.2		0.54	0.04		
>0.2 $\mu\text{m}^*$	23 $\pm$ 1	41 $\pm$ 3	1.3 $\pm$ 0.2	31 $\pm$ 4	0.48	0.10	-0.06	0.11
< 0.2 $\mu\text{m}$	34 $\pm$ 1	59 $\pm$ 2	3.0 $\pm$ 0.1	69 $\pm$ 3	0.59	0.04	0.05	0.06
> 30 kDa*	nd.	nd.	3.5 $\pm$ 0.2	81 $\pm$ 5	0.53	0.04	-0.01	0.05
< 30 kDa	2.03 $\pm$ 0.04	3.5 $\pm$ 0.1	0.83 $\pm$ 0.03	19 $\pm$ 1	0.80	0.03	0.26	0.05
> 5 kDa*	nd.	nd.	3.9 $\pm$ 0.2	88 $\pm$ 5	nd.	nd.	nd.	nd.
< 5 kDa	<LOD	nd.	0.50 $\pm$ 0.02	11 $\pm$ 1	nd.	nd.	nd.	nd.
0.2 $\mu\text{m}$ - 30 kDa*	32 $\pm$ 1	56 $\pm$ 2	2.2 $\pm$ 0.1	50 $\pm$ 3	0.57	0.04	0.03	0.05
30 -5 kDa*	nd.	nd.	0.33 $\pm$ 0.03	7.5 $\pm$ 0.8	nd.	nd.	nd.	nd.

DOC: dissolved organic carbon. \*: Calculated fraction. <LOD: below limit of detection. nd.: not determined.

**Table 7** - Chemical and isotopic compositions of filtrates and ultrafiltrates for the OM deposition experiment.

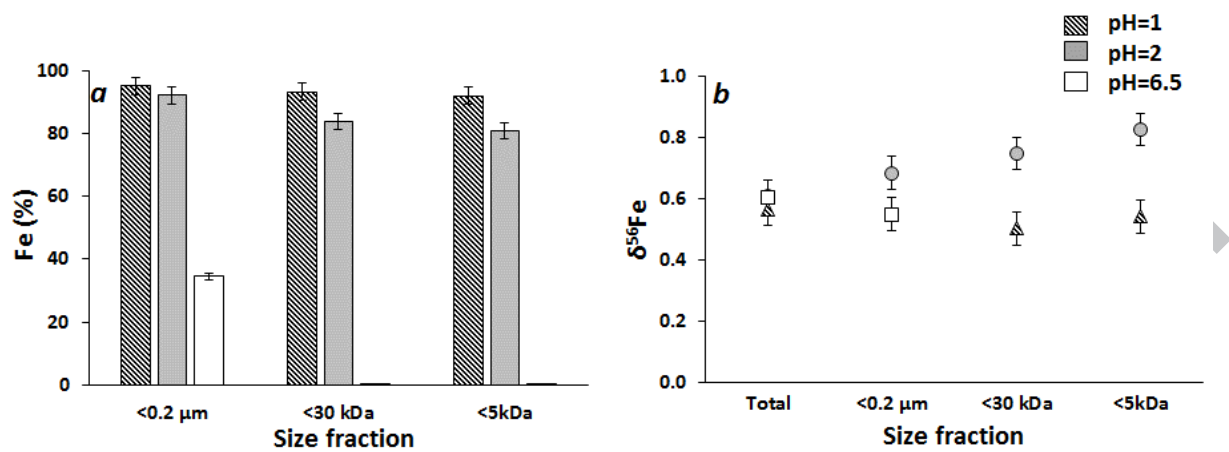
OM deposition pH 2								
Size fraction	[Fe] $\mu\text{mol L}^{-1}$	[Fe] (%)	DOC $\text{mmol L}^{-1}$	DOC (%)	$\delta^{56}\text{Fe}$ (‰)	2 $\sigma$ (‰)	$\delta^{56}\text{Fe}'$ (‰)	2 $\sigma'$ (‰)
Total	53 $\pm$ 1		4.1 $\pm$ 0.1		0.63	0.04		
> 0.2 $\mu\text{m}^*$	29 $\pm$ 1	55 $\pm$ 3	2.8 $\pm$ 0.1	69 $\pm$ 4	0.61	0.08	-0.02	0.09
< 0.2 $\mu\text{m}$	24 $\pm$ 1	45 $\pm$ 2	1.3 $\pm$ 0.04	31 $\pm$ 1	0.65	0.04	0.02	0.06
> 30 kDa*	45 $\pm$ 1	86 $\pm$ 3	3.8 $\pm$ 0.1	92 $\pm$ 5	0.62	0.04	-0.01	0.06
< 30 kDa	7.6 $\pm$ 0.2	14.3 $\pm$ 0.4	0.32 $\pm$ 0.01	7.8 $\pm$ 0.4	0.68	0.04	0.05	0.06
> 5 kDa*	46 $\pm$ 1	87 $\pm$ 3	3.8 $\pm$ 0.1	92 $\pm$ 5	0.66	0.04	0.03	0.06
< 5 kDa	6.9 $\pm$ 0.1	13.1 $\pm$ 0.4	0.32 $\pm$ 0.01	7.7 $\pm$ 0.4	0.40	0.04	-0.23	0.06
0.2 $\mu\text{m}$ - 30 kDa*	16.2 $\pm$ 0.7	31 $\pm$ 1	0.94 $\pm$ 0.05	23 $\pm$ 1	0.64	0.06	0.01	0.07
30 -5 kDa*	0.6 $\pm$ 0.2	1.2 $\pm$ 0.4	0.003 $\pm$ 0.016	0.1 $\pm$ 0.4	3.73	1.34	3.10	1.34
OM deposition pH 6.5								
Size fraction	[Fe] $\mu\text{mol L}^{-1}$	[Fe] (%)	DOC $\text{mmol L}^{-1}$	DOC (%)	$\delta^{56}\text{Fe}$ (‰)	2 $\sigma$ (‰)	$\delta^{56}\text{Fe}'$ (‰)	2 $\sigma'$ (‰)
Total	48 $\pm$ 1		4.4 $\pm$ 0.2		0.52	0.04		
>0.2 $\mu\text{m}^*$	43 $\pm$ 1	89 $\pm$ 3	1.3 $\pm$ 0.2	23 $\pm$ 4	0.56	0.04	-0.06	0.05
< 0.2 $\mu\text{m}$	5.2 $\pm$ 0.2	10.8 $\pm$ 0.4	3.0 $\pm$ 0.1	77 $\pm$ 4	0.18	0.04	-0.35	0.06
> 30 kDa*	nd.	nd.	3.7 $\pm$ 0.2	84 $\pm$ 5	nd.	nd.	nd.	nd.
< 30 kDa	<LOD	nd.	0.71 $\pm$ 0.02	16 $\pm$ 1	nd.	nd.	nd.	nd.
> 5 kDa*	nd.	nd.	4.2 $\pm$ 0.2	93 $\pm$ 5	nd.	nd.	nd.	nd.
< 5 kDa	<LOD	nd.	0.29 $\pm$ 0.01	6.6 $\pm$ 0.3	nd.	nd.	nd.	nd.
0.2 $\mu\text{m}$ - 30 kDa*	nd.	nd.	2.7 $\pm$ 0.1	61 $\pm$ 3	nd.	nd.	nd.	nd.
30 -5 kDa*	nd.	nd.	0.41 $\pm$ 0.03	9.3 $\pm$ 0.7	nd.	nd.	nd.	nd.

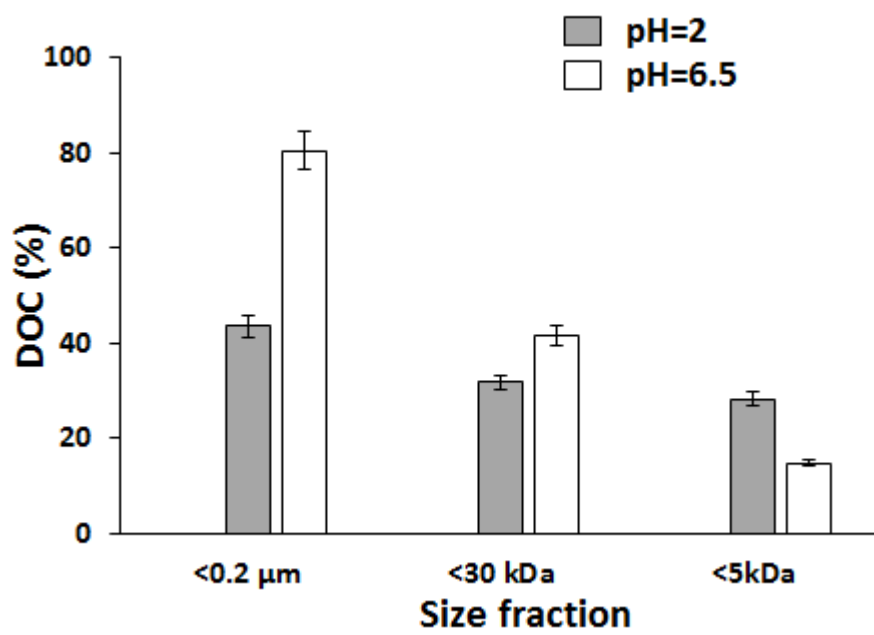
DOC: dissolved organic carbon. \*: Calculated fraction. <LOD: below limit of detection. nd.: not determined.

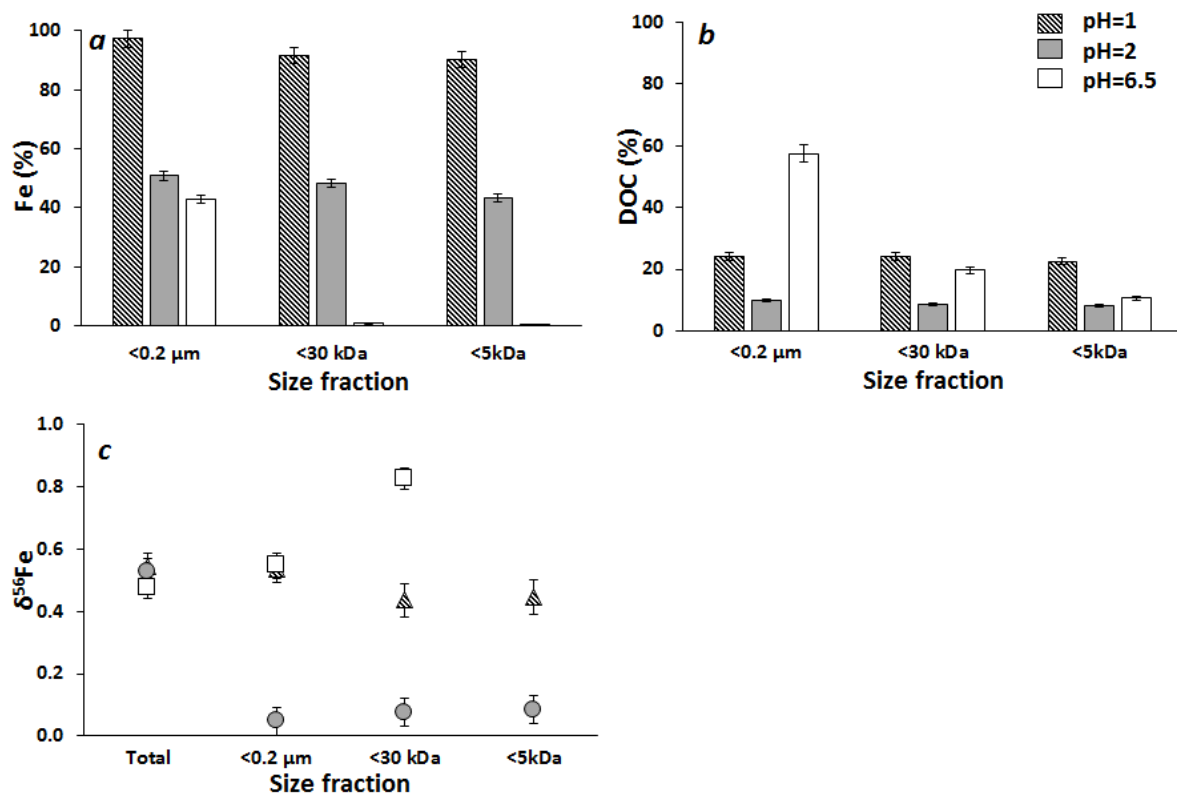
**Table 8** - Chemical and isotopic compositions of filtrates and ultrafiltrates for the Fe-OM natural association.

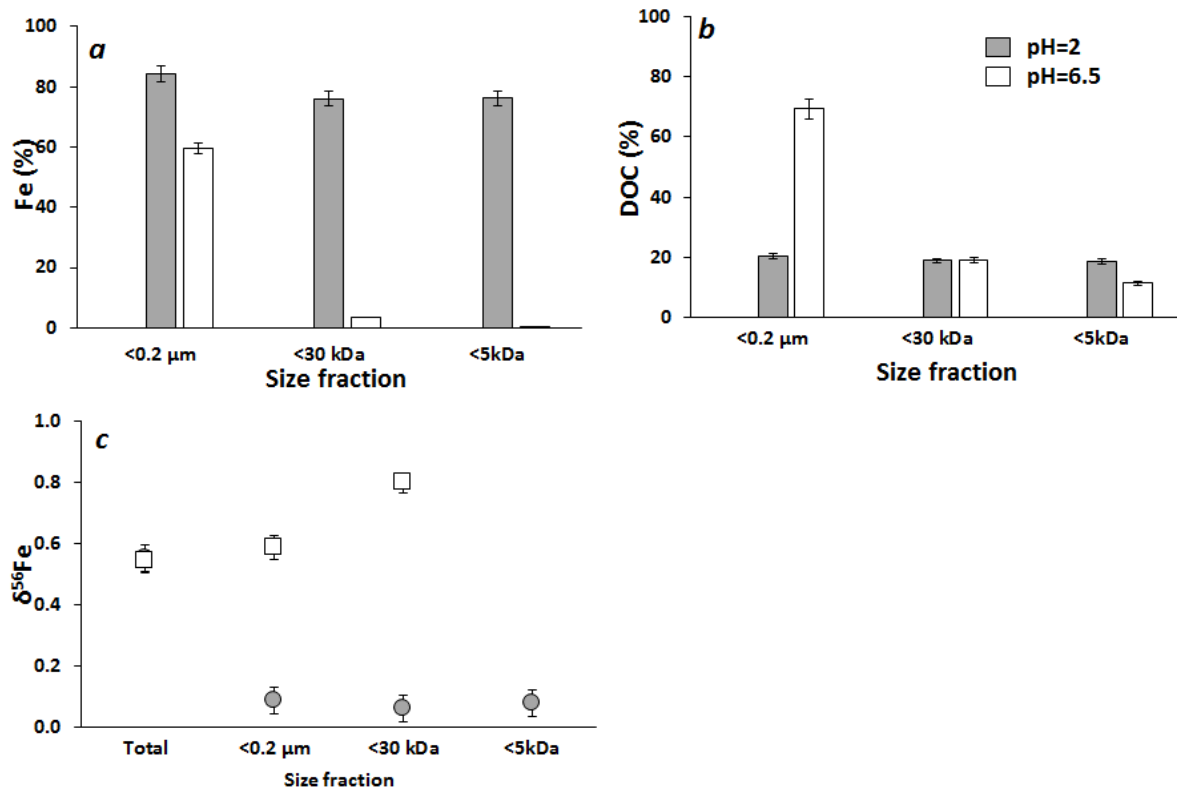
Fe -OM natural association								
Size fraction	[Fe] $\mu\text{mol L}^{-1}$	[Fe] (%)	DOC $\text{mmol L}^{-1}$	DOC (%)	$\delta^{56}\text{Fe}$ (‰)	2 $\sigma$ (‰)	$\delta^{56}\text{Fe}'$ (‰)	2 $\sigma'$ (‰)
Total	3945 $\pm$ 60		8.4 $\pm$ 0.2		0.17	0.03		
> 5 $\mu\text{m}$	406 $\pm$ 7	11.6 $\pm$ 0.3	0.85 $\pm$ 0.02	10.2 $\pm$ 0.4	0.32	0.04	0.15	0.04
< 5 $\mu\text{m}^*$	3089 $\pm$ 61	88 $\pm$ 2	7.5 $\pm$ 0.2	90 $\pm$ 4	0.15	0.03	-0.02	0.04
5-0.2 $\mu\text{m}^*$	1634 $\pm$ 10	47 $\pm$ 1	2.01 $\pm$ 0.02	24 $\pm$ 1	0.16	0.03	-0.01	0.04
< 0.2 $\mu\text{m}^*$	1455 $\pm$ 62	42 $\pm$ 2	5.5 $\pm$ 0.2	66 $\pm$ 3	0.15	0.05	-0.02	0.06
0.2 $\mu\text{m}$ - 30 kDa	1229 $\pm$ 21	35 $\pm$ 1	2.7 $\pm$ 0.1	32 $\pm$ 1	0.06	0.03	-0.11	0.04
< 30 kDa	234 $\pm$ 4	6.7 $\pm$ 0.2	2.8 $\pm$ 0.1	34 $\pm$ 1	0.34	0.03	0.17	0.04
30 -5 kDa*	216 $\pm$ 4	6.2 $\pm$ 0.2	1.7 $\pm$ 0.1	21 $\pm$ 1	0.34	0.03	0.17	0.04
< 5 kDa	18.4 $\pm$ 0.3	0.53 $\pm$ 0.01	1.10 $\pm$ 0.03	13.2 $\pm$ 0.5	0.40	0.07	0.23	0.08

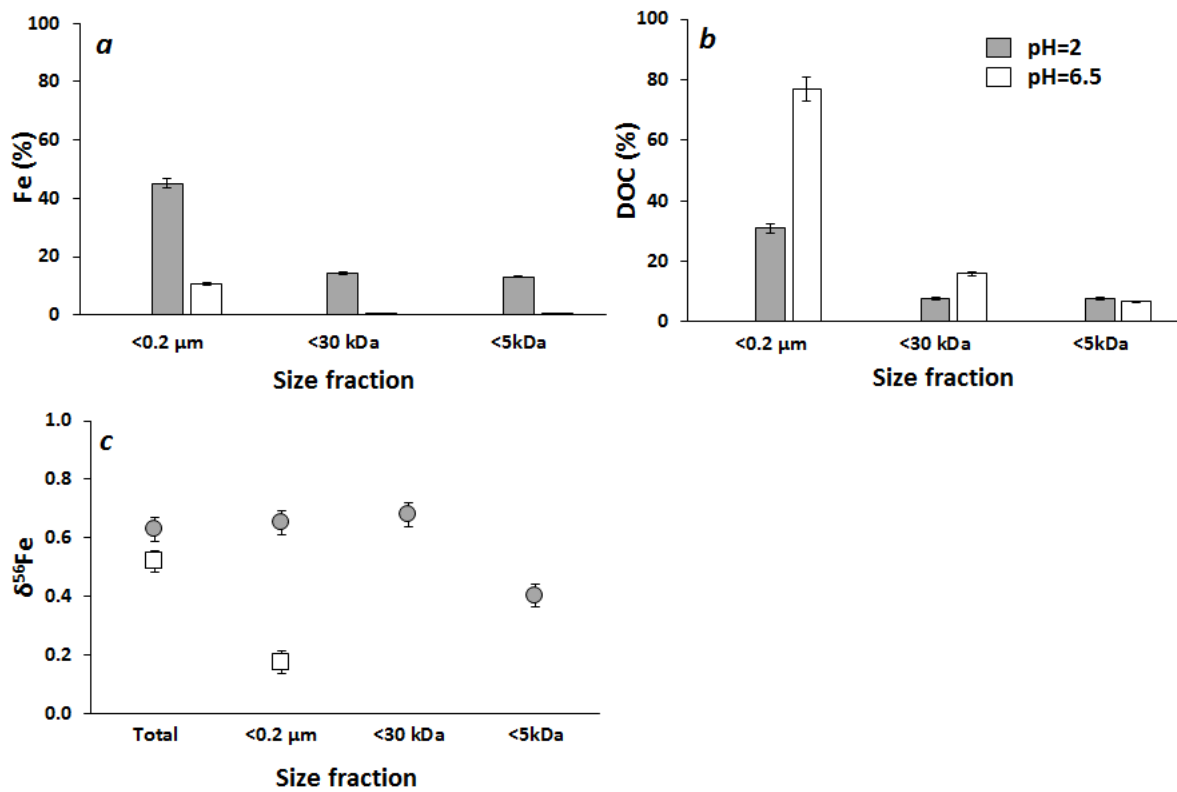
DOC: dissolved organic carbon. \*: Calculated fraction.

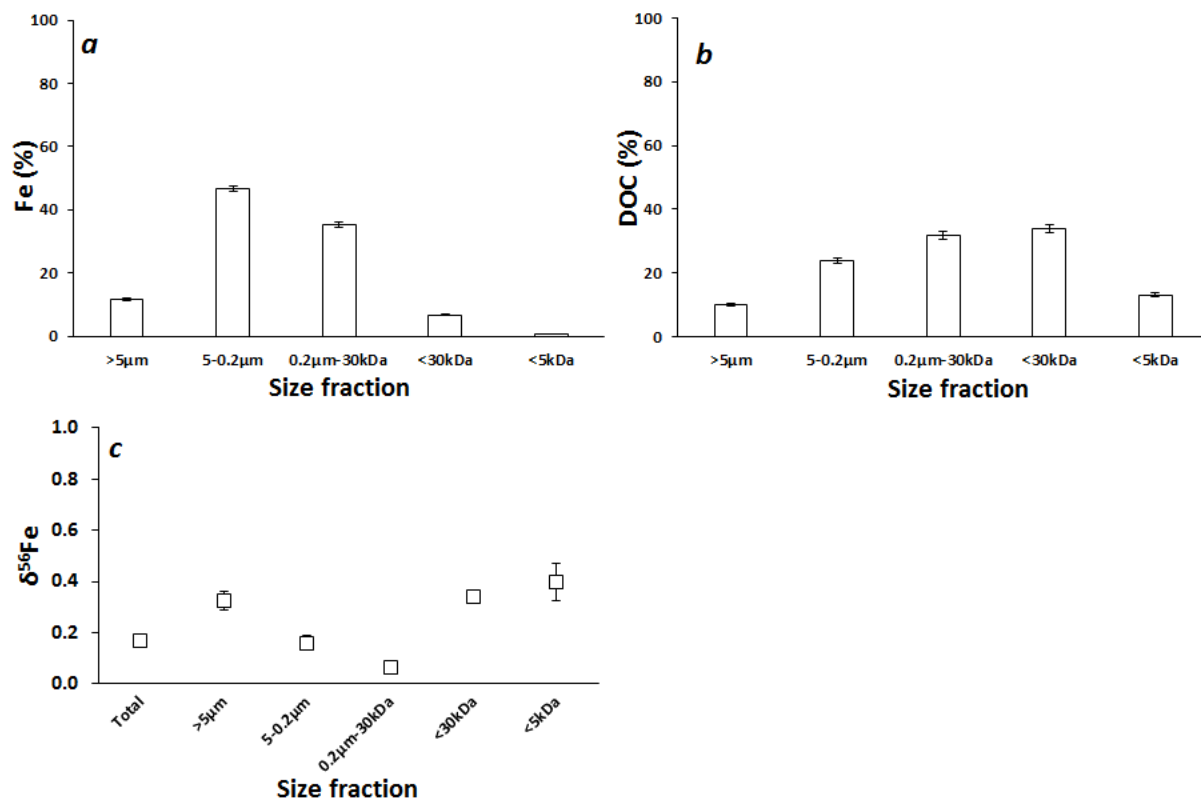


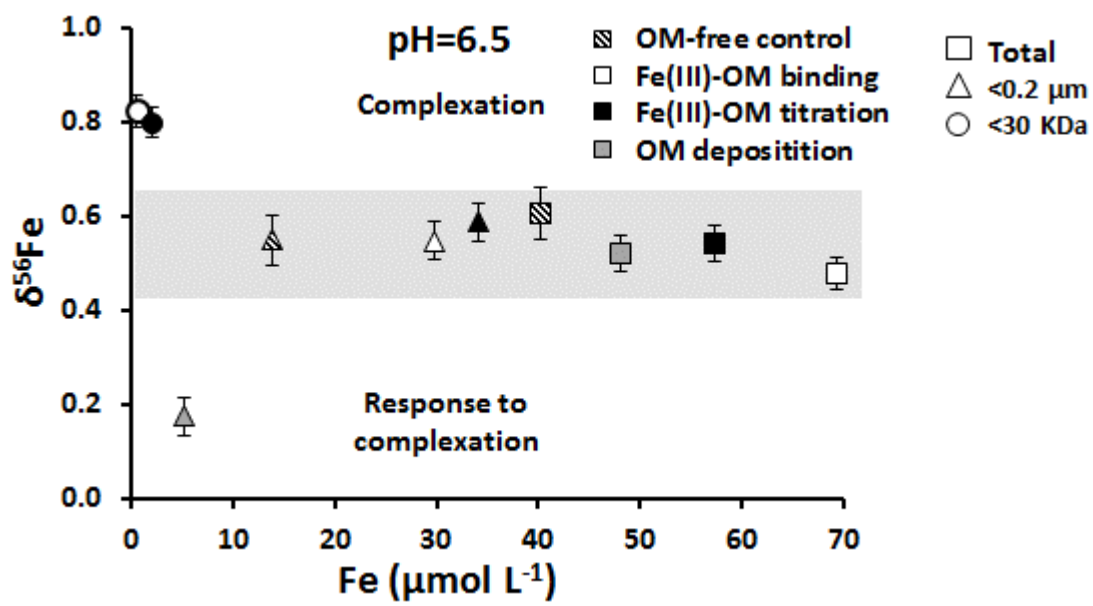


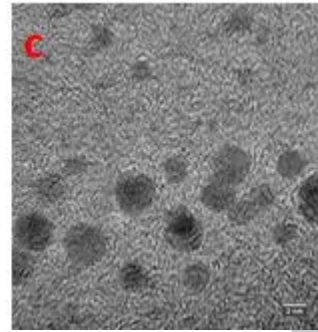
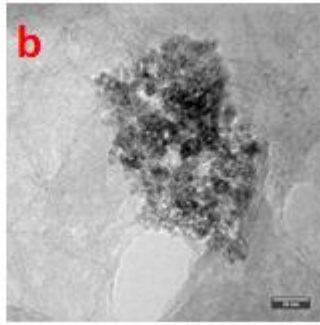
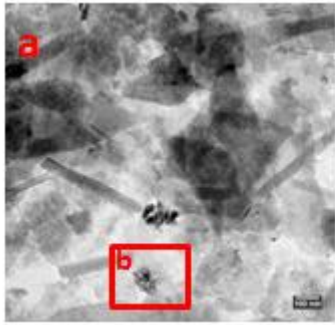




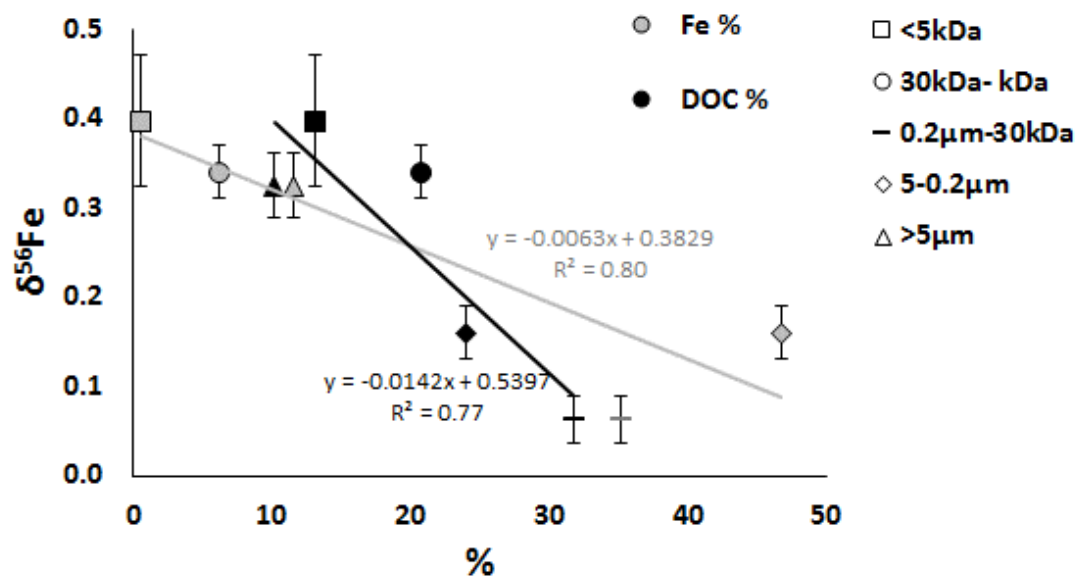








ACCEPTED MANUSCRIPT



ACCEPTED MANUSCRIPT